INVESTIGATION OF REMAINING SATURATION FROM GAS GRAVITY DRAINAGE BASED ON TIME LAPSE X-RAY CT TOMOGRAPHY WITH APPLICATION IN NATURALLY FRACTURED RESERVOIRS

A Thesis

by

ERICK RAFAEL MARTINEZ ANTUNEZ

Submitted to the Office of Graduate and Professional Studies of
Texas A&M University
in partial fulfillment of the requirements for the degree of

MASTER OF SCIENCE

Chair of Committee,	David S. Schechter
Committee Members,	Berna Hascakir
	Judith Chester
Head of Department,	Daniel Hill

December 2016

Major Subject: Petroleum Engineering

ABSTRACT

Naturally fractured reservoirs (NFR) represent an important fraction of oil reserves in the world. In many of the NFR, significant volumes of oil have been or are expected to be recovered from the matrix due to the presence of the gas gravity drainage drive mechanism. Nonetheless, there are some uncertainties to accurately predict oil recovery factors and remaining fluids saturations due to this drive mechanism despite the existence of studies performed in the last three decades.

Several mathematical models for gravity drainage in NFR have been developed based on results obtained from laboratory experiments. However, these models have not provided accurate results in field applications. One of the reasons is that the experiments only considered an oil-gas system which in many cases is not a realistic assumption due to the presence of connate water in the reservoirs. Another reason is that, in some cases, heterogeneities, such as vuggy porosity, were ignored in both the experiments and the mathematical models.

Based on these considerations, two long-term experiments that mimicked gas gravity drainage in NFR were performed. The experiments were carried out with the purpose of acquiring data that might be used to improve current mathematical models or to develop new ones. During the experiments, time-lapse X-Ray CT images were acquired at different intervals with the objective of determining the fluids saturation along the core samples due gravity drainage. Additionally, oil produced was measured.

Experiment 1 was performed in an oil-brine-air system. A stack of six Berea sandstone core samples in capillary contact was used. Initially, the stack was saturated with oil at irreducible water saturation.

Experiment 2 was performed in an oil-air system. A one-piece of Edwards limestone core with primary and vuggy porosity core was used. At the initial condition, the core was saturated with oil. Due to the presence of vugs, a novel technique was developed to quantify porosity and oil saturation for the primary porous system and the vuggy porous system.

For both experiments, a good match between the measured oil produced and the remaining oil volume in the matrix estimated from the remaining fluids saturations obtained through the CT X-Ray images was observed. The techniques used in these experiments provide a new, unique and reliable method to study the important phenomenon of gas gravity drainage in NFR.

DEDICATION

This thesis is dedicated to my wife, Beatriz, and to my children, Erick Augusto and Renata, for all the love and support they have provided me.

ACKNOWLEDGEMENTS

I would like to thank my committee chair, Dr. David Schechter, who took me as his student, served as the greatest mentor, and supported me throughout my graduate studies at Texas A&M University.

I would like also to thank Dr. Berna Hascakir and Dr. Judith Chester for serving as my committee members and for their invaluable comments.

I would like to thank the Petroleum Engineering Department at Texas A&M University for giving me the opportunity to achieve this goal. Thanks also go to my friends, colleagues, faculty and staff for making my time at Texas A&M University a great experience. Special thanks go to Mr. John Maldonado, facilities coordinator at the Harold Vance Department of Petroleum Engineering, for all the support provided to design and construct the apparatus used in the experiments of this thesis.

I would like to extend my gratitude to PEMEX and CONACyT for their financial support and for giving me the opportunity to pursue a master degree at Texas A&M University.

Finally, thanks to my parents, my sisters, and my in-laws for all their encouragement, support, patience, and love.

NOMENCLATURE

a	Klein-Nishina coefficient
CT	CT number
$CT_{a,o,w}$	CT number of air, oil or water
$CT_{ar,or,wr}$	CT number of rock saturated with air, with oil or with water
CT_{aor}	CT number of rock saturated with air and oil
CT_{awor}	CT number of rock saturated with air, oil, and water
d	Diameter
dh	Distance along the trajectory length
E	Energy level
h	Thickness
h(x,y)	Coordinates of the attenuation coefficient in two dimensions
I	Intensity remaining
I_0	Incident X-Ray intensity
L	Trajectory length
m_{wet}	Weight of rock saturated with brine
m_{dry}	Weight of rock saturated with air
Np	Total cumulative oil produced
Np_{CT}	Cumulative oil produced from the matrix estimated by CT data
Np_{ncv}	Cumulative oil produced recovered from the non-touching vugs
Np_m	Cumulative oil produced recovered from the matrix

Np_{vol}	Cumulative oil produced from the matrix
n	Number of elements into the region of interest
ROI	Region of interest
S_o	Oil saturation
S_{oncv}	Oil saturation in non-touching vugs
S_w	Water saturation
S_{wi}	Irreducible water saturation
Vo_i	Initial oil volume obtained by CT
Vo_{CT}	Oil volume obtained from CT
Vo_{cv}	Initial oil volume contained in the touching vugs
Voi_{ncv}	Initial oil volume in non-touching vugs
Vo_{ncv}	Remaining oil volume in the non-touching vugs
Vo_f	Volume contained in the fracture
V_p	Pore volume
V_b	Bulk volume
TNCV	Total number of vuggy touching cells
TNIV	Total number of vuggy non-touching cells
TROI	Total number of cells
Φ	Porosity
μ	Linear attenuation coefficient
μ_w	Linear attenuation coefficient of water

TABLE OF CONTENTS

Page

LIST OF FIGURES

Page

LIST OF TABLES

Page

CHAPTER I

INTRODUCTION

Naturally fractured reservoirs (especially carbonate reservoirs) typically show a high heterogeneity reflected on their porosity and permeability distributions. If diagenetic events are present (e.g. dissolution), heterogeneity becomes higher giving way to complex porous systems which exhibit different scales.

At early stages of the life cycle of a naturally fractured reservoir, the production performance relies heavily on energy issues such as the expansion of the rock-fluids system or a waterdrive due the presence of an active aquifer. However, when this type of reservoir comes to its maturity phase, production performance is controlled principally by the effects that heterogeneity provokes on the transport of fluids along the reservoir and to the wells. At this stage, the heterogeneity effects are more evident if the reservoir is under the influence of an aquifer or a gas cap (formed naturally or by gas injection).

For thick naturally fractured reservoirs with a gas cap, one of the primary and most efficient drive mechanisms that influence the production performance is gravity drainage (GD). If gravity drainage is present, the way the reservoir is managed will determine largely the final recovery factor. Nevertheless, to settle the best strategic actions (supported on GD) that contribute to maximizing the recovery factor, it is necessary to quantify the volume that can be obtained due to this mechanism and the time that may take to recover it.

In the last 30 years, several models have been created to predict oil production rates and oil recovery factors due to gravity drainage. However, most of those models have been created for single-porosity reservoirs leaving aside the possibility to include heterogeneity effects due to the presence of additional porous systems such as fractures or vugs.

For naturally fractured reservoirs under gravity drainage drive mechanism, few mathematical models have been developed. As in models created for single porosity reservoir, these models closely matched oil production recovered by gravity drainage in experiments that mimicked a naturally fractured reservoir in a two-phase system. However, distribution of fluids along the rock is not described for those developed models either the nature of the mathematical model or the lack of experimental data. Additionally, most of those models of those models have not provided accurate results in field applications. One on the reasons is that experiments used to develop the mathematical models only consider the presence of two phases (oil and gas) which in many cases is not a realistic assumption.

On the other hand, developed models for gravity drainage in naturally fractured reservoir did not consider the presence of secondary porosity such as vuggy porosity.

I.1 Objectives and Scope

The objective of this thesis is to perform two experiments that mimic immiscible gravity drainage drive mechanism in a naturally fractured reservoir. The experiments are performed at ambient conditions in whole core rock samples with the purpose of acquiring

data that might be used to improve current mathematical models or to develop new ones. During the experiments, oil produced due to gravity drainage is measured volumetrically. Additionally, time-lapse X-Ray CT images are acquired at different intervals with the purpose of determining the distribution of fluid saturation along the core samples. Each experiment is executed under different conditions:

- Experiment 1 emulates gravity drainage in a naturally fractured reservoir in a three-phase system: oil, gas, and immobile water (water at irreducible saturation).
- Experiment 2 emulates gravity drainage in a naturally fractured reservoir where the matrix exhibits vuggy porosity, in a system two-phase system: oil and gas.

I.2 Overview of Thesis Chapters

This thesis is divided into five chapters. The next chapter presents notorious investigations of gravity drainage in naturally fractured reservoir. Chapter III describe theory background about the application of X-Rays CT Images to characterize porous system and distribution of fluids contained in a rock. Chapter IV present the results obtained during the execution of the two experiments previously described. The last chapter summarizes the work and presents the conclusions and future work and recommendations.

CHAPTER II

GRAVITY DRAINAGE STUDIES IN NATURALLY FRACTURED RESERVOIRS

Gravity drainage has been investigated from the 35 years. Hagoort (1980) conducted a series of experiments based on centrifugal displacement to determine the oil phase relative permeability for gravity drainage in a gas-oil system under the presence of connate water saturation in four different not-fractured water-wet rock samples. Results indicated very low remaining oil saturation at the end of the experiments for all the analyzed rock samples concluding that gravity drainage can be an efficient process in water-wet systems. Additionally, taken as a basis the classic Buckley and Leverett theory (Buckley and Leverett. 1942), he developed a mathematical approximation to evaluate the potential of gravity drainage as a function of time and oil relative permeability for a not-fractured reservoir.

An analytical model for naturally fractured gas-condensate reservoirs was developed by Castelijns and Hagoort (1984). Modeling of released condensate from the matrix to the fracture system was based on the disequilibrium between oil gravity head and capillary pressure. Trapped oil volumes in the matrix system were assumed due to capillary rise and reservoir geometry whereby, according to this assumption, gas will never fully displace oil from the matrix by gravity drainage unless oil-gas capillary pressure is equal to zero. Moreover, not only oil expelled from the matrix to the fractures were considered but also reimbibition (reinfiltration caused by oil moving from fractures

to matrix due capillary pressure) were included. The model was applied to the Waterton reservoir through the evaluation of condensate accumulations in the matrix and fracture systems. It was found that reinfiltration occurred and cannot be neglected during gravity drainage.

Firoozabadi and Markeset (1994) conducted an experiment to investigate the influence of the fracture-liquid transmissibility in the flow of the oil phase for a reservoir under the effect of gravity drainage. Rock blocks with different permeabilities were vertically stacked incorporating different sets of spacers between them with the objective to emulate a natural fracture. The rock blocks were saturated with normal decane; air was utilized as the gaseous phase. They found that fracture apertures had a high influence on the oil flow: large fracture apertures caused low rates of drained oil while small fracture apertures provoked higher rates. In this experiment, oil recovered due gravity drainage was reported, but they did not describe the distribution of fluids along the rock samples used. An extension of their previous experimental work was conducted to study the effect of inclination on the crossflow (oil drained from a certain matrix block to the fracture system and then reinfiltrated into another matrix block) in layered rock slabs (Firoozabadi and Markeset. 1992). The results obtained from this study revealed that inclination affected highly the crossflow among the rock blocks (i.e. the higher inclination, the lower oil recovered due drainage).

Based on Darcy's Law and film theory, Schechter and Guo (1996) proposed a mathematical model for free-fall gravity drainage in naturally fractured reservoirs. The model was compared against a series of laboratory experiments that mimicked free-fall

gravity drainage. It was found that a match of the experimental results (e.g. produced oil produced by gravity drainage versus time) was improved through their proposed model compared to models previously developed by Dykstra (1978), Cardwell and Parsons (1949), Pavone et al. (1989) and Luan (1994). The reason for the poor matching quality on the compared models lies on the unrealistic assumptions that were taken as a theoretical basis. Along with free-fall gravity drainage experimental work and its mathematical modeling, it was conducted an experimental analysis for gravity drainage under non-equilibrium conditions by the continuous injection of CO2 as the displacer phase. Results of the experiments under non-equilibrium conditions were reproduced through a simulation model built on the developed model and the incorporation of molecular diffusion between the gas and liquid phases. They concluded that, in low permeability reservoirs, the molecular diffusion is the dominant mechanism of recovery leaving aside gravity drainage, and vice versa. A description of the fluid distribution along the rock sample was not reported in this experimental work.

In the same manner, as occurs in single porosity reservoirs, numerical simulation is a widely used tool for modeling, understanding, and predicting the behavior of a naturally fractured reservoir. One of the key elements in numerical simulation that take place in the modeling of transport of fluids for this type of reservoir is the matrix-fracture transfer function. This function describes the interchange of fluids that occurs at the interface of the block matrix and the fracture system. Reliability on the dynamic performance of a naturally fractured reservoir obtained by numerical simulation (especially on those parameters that describe the changes of the volumes allocated in the

matrix-fracture system and the velocity at which occurs) will be determined by an appropriate formulation of the matrix-fracture transfer function. For the case of numerical simulation of fractured reservoirs under gravity drainage mechanism, this function becomes particularly important.

Since the past five decades, many formulations for the matrix-fracture function have been published. Miguel-H et al. (2004) made a comparison of the matrix-fracture transfer function proposed by Kazemi et al. (1976), Litvak (1985), Sonier et al. (1988), Quandalle and Sabathier (1989), Beckner et al. 1987 and Bech et al. (1991). Those transfer functions were implemented in a numerical simulation model with the main objective of analyzing the effect that each one of them provokes over the rate of change of oil saturation in matrix blocks for a naturally fractured reservoir under fully-vertical gas gravity drainage. From the comparison, they observed that formulation of Bech et al. (1991) had the better representation of the movement of gas and oil phases between the matrix and the fracture systems. Besides the previous conclusion, they conducted an analysis focusing on the direction of the flow of oil displaced from matrix block due gravity drainage. It was found that oil flows vertically downwards (lateral flow is neglected) from the matrix to the fracture system if the bottom face of the matrix block is opened at least 75% of its area. Opened area less than 75% at the lower face will restrict the vertical flux causing that oil moves out through the lateral faces of the matrix block. Additionally, they simulated the experiment reported by Firoozabadi (1993) using a commercial simulator which utilizes a slight modification of the transfer function presented by Bech et al. (1991). The obtained results show a regular-quality matching.

Ladron et al. (2009) proposed a new formulation for representing the exchange of fluids between matrix block and fracture for an oil-gas system. They take as a basis the matrix-fracture transfer function developed by Kazemi et al. (1976) which only takes into account viscous forces. Capillary effects were included in their formulation by incorporating two explicit terms that describe the oil fluxes matrix-fracture and fracture-matrix (i.e. drainage and reinfiltration). They performed a numerical simulation of the gravity drainage mechanism over a stack of matrix blocks separated by fractures. Results obtained by the proposed formulation were contrasted against two commercial simulators. It was observed that commercial simulators had poor results compared to their proposed model. However, measurements of the quality of the obtained results were based on another numerical simulation study and not based on an experimental study.

CHAPTER III

FLUID DISTRIBUTION TRACKING IN ROCK SAMPLES THROUGH X-RAY CT TOMOGRAPHY

III.1 Basic Principles

Computerized Tomography is an imaging technique based on the emission of X-Rays around an object. When an object is CT scanned, a 2-dimensional image (CT slice) is obtained; this image is composed of a set of volumetric elements (voxels) that show the attenuation in the energy of the X-Rays that have passed through the scanned object at a given position (Figure 1). Then, a 3-dimensional representation of the scanned object can be constructed by a series of CT slices taken at different positions over the object length.

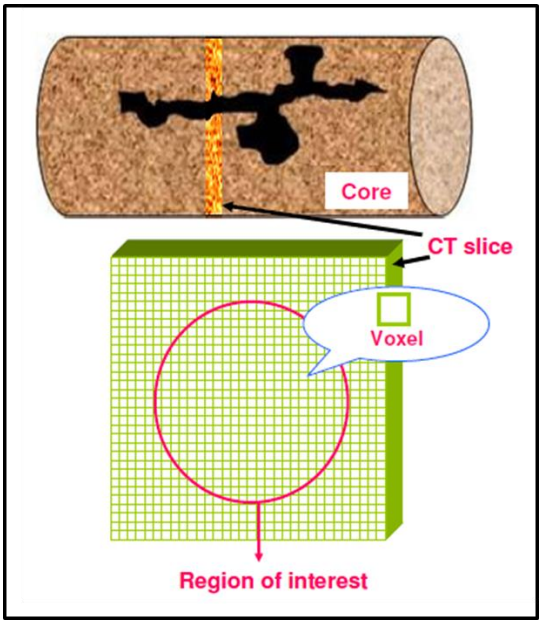

Figure 1. CT images representation (Izgec and Hill 2010)

From the Figure 1, we can note that images obtained from CT scanner are squared planes composed of a determined number of voxels. However, not all voxels may have useful data. For this thesis, the concept of region of interest (ROI) presented by Izgec and Hill (2010) will be adopted to name the region of the CT images that encloses the zone where the scanned rock samples have been imaged.

In a CT scanning apparatus, a source transmits X-Rays beams at certain lever of energy (intensity) over an object. Then, a series of digital detectors records the remaining intensity of the X-Rays that have passed through the object (Figure 2). The change of the intensity of the X-Rays is accounted into a parameter called attenuation coefficient μ.

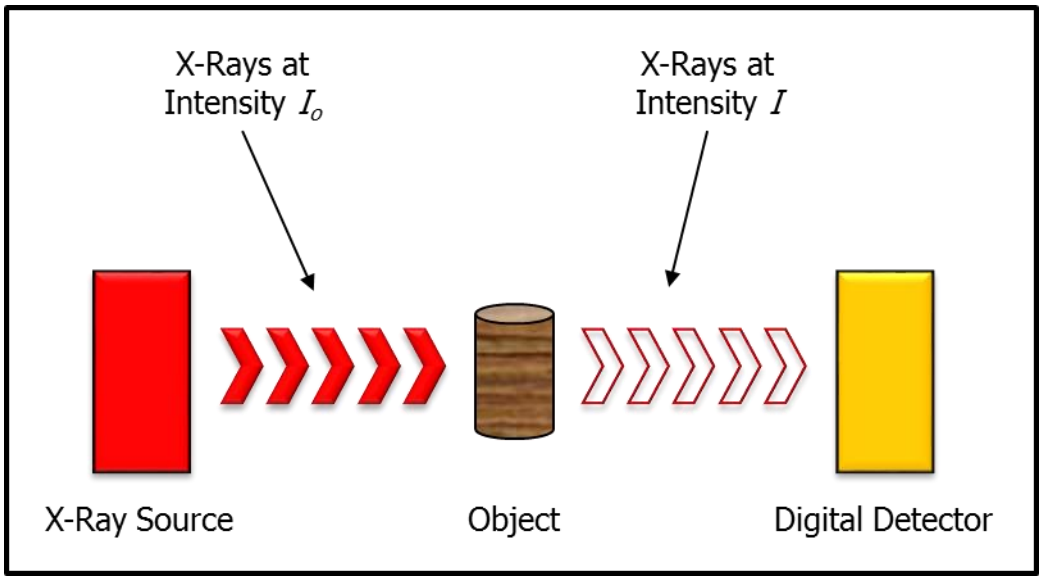

Figure 2. Schematic representation of CT scanning

For each volumetric element that is included in a CT slice, the linear attenuation coefficient is defined by Beer's Law (Akin and Kovscek. 2003) as follows:

$$I = I_0 \cdot e^{-\mu h} \tag{3.1}$$

where I is the intensity remaining after the transmitted X-Ray passes through a homogeneous object with thickness h, I_0 is the incident X-Ray intensity and μ is the linear attenuation coefficient.

The attenuation of the X-Rays is dependent on the atomic number Z and electron density (bulk density) ρ of the scanned substance, therefore, different substances have their characteristic linear attenuation coefficient μ. If the scanned object is constituted of different materials, the energy emitted along a given X-Ray trajectory is:

$$\ln\left(\frac{I}{I_0}\right) = \int_o^L \mu\big(h(x,y)\big)dh \tag{3.2}$$

where $h(x,y)$ are the co-ordinates of the attenuation coefficient in two dimensions, L is the trajectory length from the X-Ray source to the detector, and dh is a distance along the trajectory length.

CT images show the attenuation coefficient transformed into a parameter called CT number. This transformation is performed by the normalization of the measured attenuation coefficient with the coefficient of a standard fluid. Usually, water attenuation coefficient is utilized as standard fluid. Thus, CT number is defined as follows (Akin and Kovscek. 2003):

$$CT = 1000\frac{(\mu - \mu_w)}{\mu_w} \tag{3.3}$$

where μ_w is the attenuation coefficient of water. The value of the CT number in the Eq. 3.3 is expressed in Hounsfield (H) units, where a single Hounsfield unit represents a 0.1% of change in density with respect to the fluid used for normalization.

Vinegar and Wellington (1987) proposed a mathematic definition of the linear attenuation coefficient as a function of bulk density and atomic number:

$$\mu = \rho\left(a + b\frac{Z^{3.8}}{E^{3.2}}\right) \tag{3.4}$$

where *a* represents the Klein-Nishina coefficient, *b* is a constant, and *E* accounts for the energy level at which X-Ray is emitted.

Particularly, for laboratory research purposes, porosity and phase distributions (i.e. phase saturations) in petroleum rock samples can be determined by using the CT number.

The porosity of a certain rock sample can be determined if the sample has been fully saturated and the scanned with two fluids that possess different densities (i.e. contrasting CT numbers). According to Withjack (1988):

$$\phi = \frac{CT_{p_1r} - CT_{p_2r}}{CT_{p_1} - CT_{p_2}} \tag{3.5}$$

where p_1 and p_2 denote the CT number for the phase 1 and the phase 2 respectively; p_1r and p_2r describe the CT number of the rock saturated with the two different phases respectively.

Air and water are two of the most popular substances used as a contrasting fluids due to the simple process required to filling a rock sample with it (Akin and Kovscek. 2003). Then, for an air-water system equation (3.5) can be written as follows:

$$\phi = \frac{CT_{ar} - CT_{wr}}{CT_a - CT_w} \tag{3.6}$$

Fluid saturations can be determined by linear interpolation (Akin and Kovscek. 2003). For an oil-water system, oil saturation is defined by:

$$S_w = 1 - S_o \tag{3.7}$$

$$S_o = \frac{CT_{wr} - CT_{owr}}{CT_{wr} - CT_{or}} \tag{3.8}$$

where the subscripts *wr*, *or*, and *owr* in Eq. 3.8 refer to the CT number of the rock sample fully saturated by water, fully saturated by oil, and saturated simultaneously with oil and water respectively.

For the case of an air-oil system saturation can be computed as follows:

$$S_a = 1 - S_o \tag{3.9}$$

$$S_o = \frac{CT_{ar} - CT_{aor}}{CT_{ar} - CT_{or}} \tag{3.10}$$

where the subscripts a*r*, *or*, and a*or* in Eq. 3.8 refer to the CT number of the rock sample fully saturated by air, fully saturated by oil, and saturated simultaneously with air and oil respectively. A different form to compute porosity and oil saturation was presented by London et al. (2014).

The process of cleaning and drying a core sample that previously has been saturated with any other substance can be very time-consuming. Considering this situation Alvestad et al. (1992) proposed an alternative way to obtain CT_{or} (CT number of the rock fully saturated with oil) by a linear interpolation of the water-saturated rock CT values,

the CT number of the dry rock sample (i.e. saturated with air), and the CT number of the pure substances:

$$CT_{or} = CT_{ar} + \frac{CT_o - CT_a}{CT_w - CT_a}\left(CT_{wr} - CT_{ar}\right) \tag{3.11}$$

For the case of a rock sample containing three type of fluids, there are different techniques to determine phase saturations (Akin and Kovscek. 2003).

One of the techniques assumes that one of the present phases is immobile (e.g. water at its irreducible saturation contained in a water-wet rock). If a phase is considered immobile, its CT number is included in the CT number of the rock sample. Then, it is assumed that CT values alterations are caused only by changes in saturation of the remaining mobile phases. According to MacAllister et al. (1993), Eq. 3.10 can be modified for a system air-oil-water (where water is immobile) by subtracting the contribution made by the irreducible water in the second term fo the numerator as follows:

$$S_o = \frac{CT_{ar} - \left[CT_{awor} - S_{wi}\left(CT_{wr} - CT_{ar}\right)\right]}{CT_{ar} - CT_{or}} \tag{3.13}$$

Equations (3.5) to (3.11) can be applied to each voxel contained in a constructed image. However, since every single voxel into the CT slice owns the same geometry and size, porosity and phase saturations also could be calculated for regions or portions (e.g. region of interest) of the imaged object by performing an arithmetic average of the CT number for the region of interest (Figure 1):

$$\overline{CT} = \sum_{i=1}^{n} \frac{CTi}{n} \tag{3.12}$$

where n denotes the total number of voxels contained in the region of interest (ROI).

Determination of porosity and fluid distribution in a rock sample based on X-Ray CT scanning is not a perfect technique and is susceptible to errors. Akin and Kovscek (2003) summarized and described four type of errors:

1. Beam hardening errors.
2. X-artefacts errors.
3. Positioning errors.
4. Machine errors.

Extended description of these errors can found in reports from Ketcham and Carlson (2001), Van Geet et al.(2001), Wellington and Vinegar (1987), and Withjack (1988).

III.2 Examples of Applications of CT Scanning in Laboratory Experiments for Naturally Fractured Reservoirs

Since X-Ray CT scanning was started to be used in laboratory experiments for the petroleum industry in 1980's, many cases have been documented where CT scanner was employed as a tool to characterize porous system in rock samples as well as to determine fluid saturations and track front movements (Akin and Kovscek. 2003). However, most of the cases where CT scanner has been used are related to studies for not naturally fractured reservoirs and just a few present applications when heterogeneities such as vugs are present. Nonetheless, there are some studies for fractured reservoirs.

Rangel-German and Kovscek (2002) performed a study of water imbibition for naturally fractured reservoirs. They executed a series of tests to understand oil expulsion from rock samples due to capillary imbibition of water. During the execution of the experiments, images of the waterfront movements were acquired through CT scans. By transforming CT number obtained from the scans at different times, the spatial distribution of oil and water along the rock sample were determined. This fluid distribution supported their presented analysis on different water imbibition behavior observed during the experiments.

Izgec and Hill (2010) presented the results of their study on matrix acidizing on vuggy carbonates reservoirs. In their study, they used high-resolution CT imaging to track the flow direction and wormholes propagation before and after acid flooding in the core samples. One of the key findings of their study based on CT imaging was that the presence of vugs induces a preferential pathway on the injected acid provoking that wormholes propagate much faster than occurs in homogeneous rock.

Moctezuma-Berthier and Fleury (2000) proposed a methodology for dual-porosity dual-permeability mapping in vuggy core samples (without the presence of natural fractures) by combining CT scanner images, nuclear resonance magnetic (NMR) relaxometry, tracer experiments, and numerical simulation. By combining those techniques they found a relation among the spatial distribution of the vugs, the contrast in the magnitude between vuggy permeability and matrix permeability, and the main path that governs the flow during the tracer experiments.

Hidajat et al. (2002) developed a technique to estimate effective permeabilities (i.e. a representative permeability of the whole porous system) on vuggy carbonates rock samples from Yates West Texas field based on CT scanner porosity mapping and NRM T2 measurements. Their technique used as an input the porosity partition estimated by CT scanner images: fraction of pore volume on the matrix system; and fraction of pore volume occupied by vug system. They found that the magnitude of the effective permeability was dominated mainly by the connectivity existing among vugs and their faction of the total pore volume.

CHAPTER IV

EXPERIMENTAL WORK AND RESULTS

Although there are many studies and analysis of fluid transport and phase distributions in naturally fractured reservoirs, gravity drainage drive mechanism has not been widely studied in laboratory when there are more than two existing phases in the matrix porous system, or when a secondary porosity (e.g. the presence of vugs) in the matrix is present.

Considering the above, two experiments have been performed with the aim of contributing to better understand gravity drainage on this type of reservoirs:

- Experiment # 1: Gravity drainage in a three-phase system where, at initial conditions, the matrix contains water at irreducible saturation (S_{wirr}) and oil at initial oil saturation ($S_{oi} = 1 - S_{wirr}$), and the fracture is fully saturated with oil. The displacer gas-phase is air. During the experiment, the oil produced due gravity drainage is registered, and CT scanner images are taken in order to determine fluid distributions along the rock samples.
- Experiment # 2: Gravity drainage in a two-phase system where, at initial conditions, rock and fracture are fully saturated with oil. The rock sample shows secondary porosity due to the presence of vugs. The displacer gas-phase is air. During the experiment, the oil produced due gravity drainage is registered, and CT scanner images are taken in order to determine fluid distributions along the rock sample.

For the experiment # 1, a stack of Berea cores in capillary contact is used to represent the matrix system. For the experiment # 2, a one-piece sample of whole core is used; this sample is not homogeneous due to the presence of vugs.

The apparatus used to measure gravity drainage performance in both experiments (Figure 3) consisted of aluminum cylindrical cell placed in vertical position; the aluminum material was selected to make the cell compatible with the CT scanner (i.e. emitted X-Rays from CT scanner can penetrate through the cell wall to the rock samples placed into it).

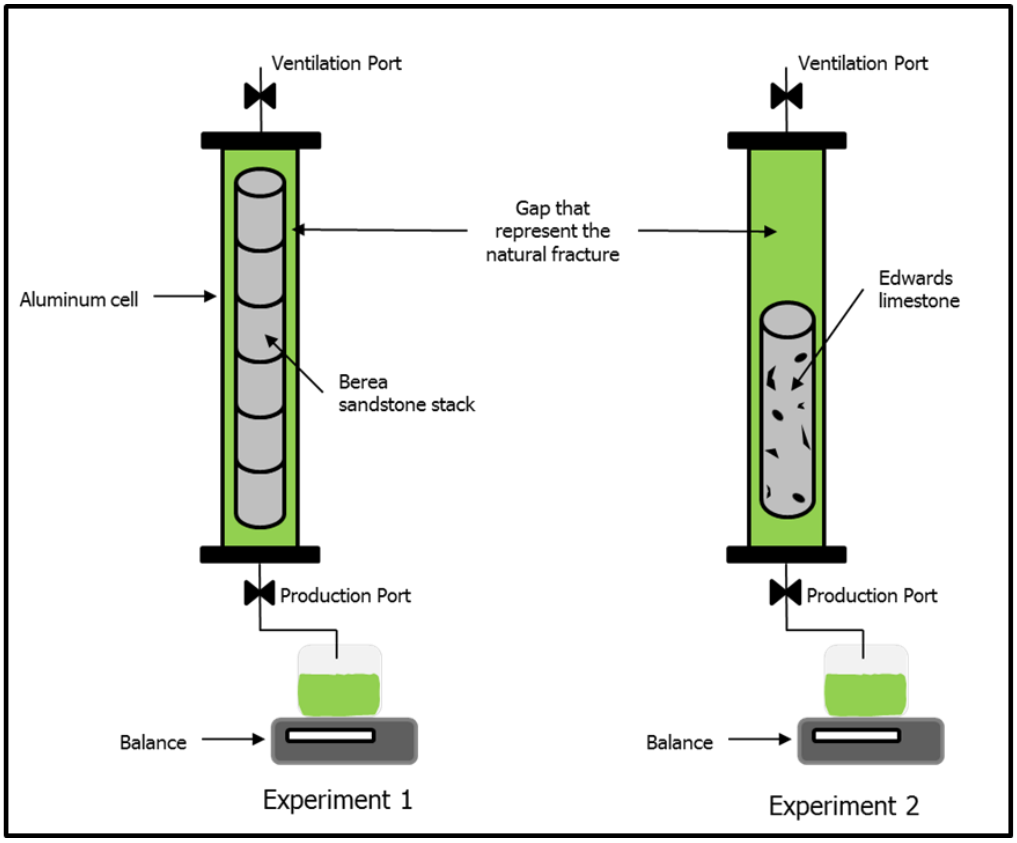

Figure 3. Gravity drainage apparatus schematics

At the time gravity drainage experiment is performed, upper and lower ports (ventilation and production respectively) are opened simultaneously. Oil drained from the rock samples is collected through a 1/8[in] diameter tubing connected to the lower port. The accumulated collected oil is measured by using a balance. At the time a CT images had to be taken, both ports were closed and the cell was taken to the CT scanner.

For both experiments, the natural fracture is represented by the existing gap between the rock samples and the interior of the cell (Figure 3). Four straight aluminum rods were attached to the cell to avoid undesirable displacements of the rock samples inside of it during the experiments (Figure 4).

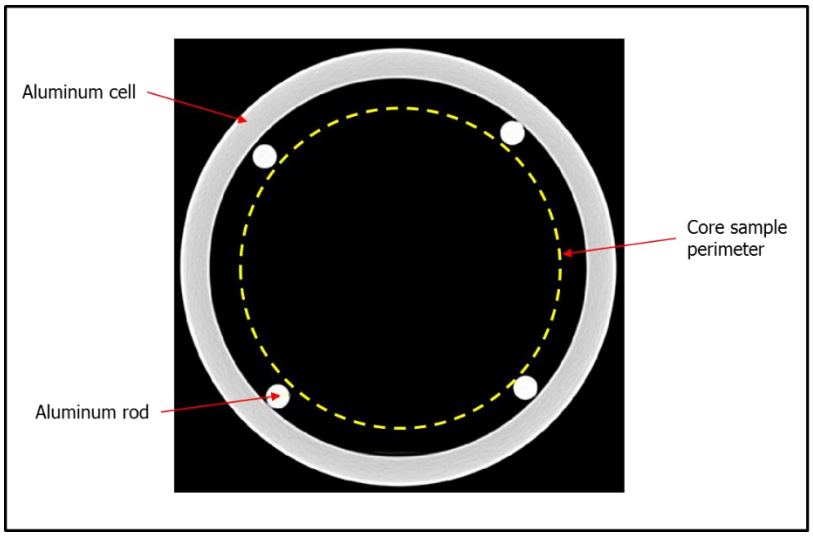

Figure 4. CT image from the gravity drainage cell

As will be discussed in later sections, dimensions of the rock samples are not the same for the two experiments. Therefore, the volume of the "fracture" is different for each case.

Figure 5 shows a flow diagram of the main steps followed to perform the gravity drainage study in both experiments. However, although it shows generic tasks, there are some differences in the execution of task 1 between the two experiments due to the nature of the rock samples and the number of phases involved on each one of them.

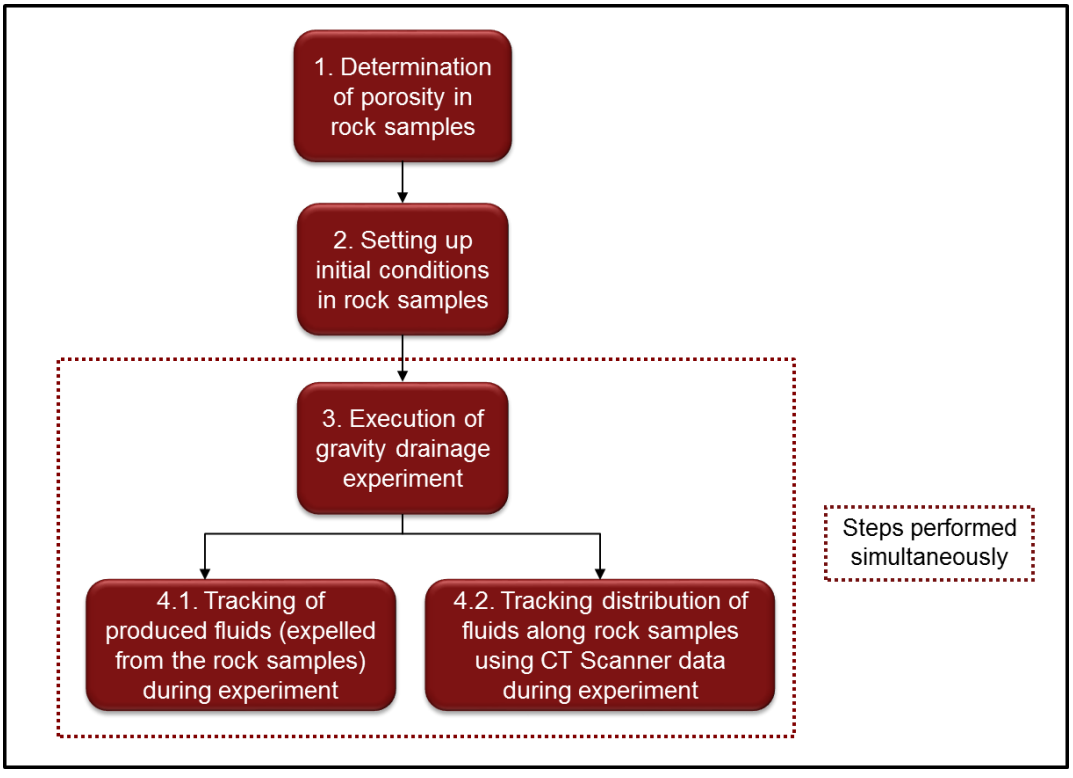

Figure 5. Experiment workflow

Details on the estimation of porosity of the rock sample in each experiment will be discussed later.

CT imaging was conducted with a 5th generation Toshiba Aquilion RXL CT Scanner. X- Ray CT scans were taken over the rock samples placed in the gravity drainage cell from the top to the bottom of it. The CT slices were collected with a separation of 1[mm] then, for the experiment 1 a total of 914 images per scan were taken; a total of 508 images per scan for the experiment 2. Every CT slice had a resolution of 512 x 512 voxels, where each voxel was a square with sides of 0.32[mm] by 0.32[mm]. Software ImageJ was used to obtain CT numbers from CT images.

IV.1 Materials

IV.1.1 Rock Samples Experiment 1

Six Berea sandstone core samples purchased from the company Cleveland Quarries were employed in this experiment. All the core samples have the same diameter and height: 101.6[mm] and 152.4[mm] respectively. With this size, rock stack on experiment 1 reaches the height of 914[mm] (Figure 6).

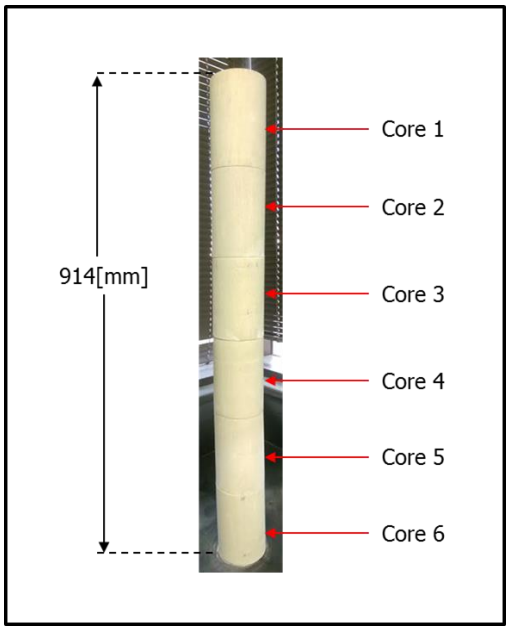

Figure 6. Berea sandstone stack

Berea sandstone has been widely used in laboratory studies in petroleum industry due to its commercial availability and, most important, due to its homogeneity. Extended description of rock properties in Berea sandstone can be found at Churcher et al. (1991) and Potts and Kuehne (1988).

CT Images were taken at different positions along the Berea cores in order to confirm their integrity (Figure 7 to Figure 12).

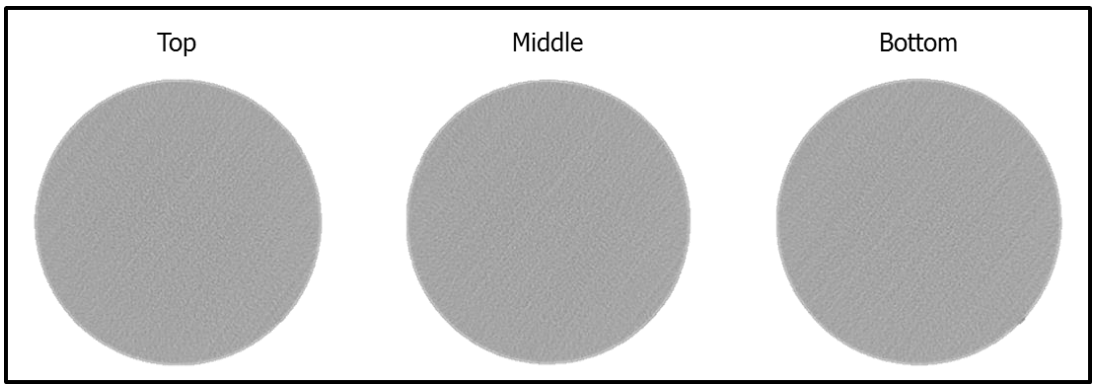

Figure 7. CT images of Berea Core # 1

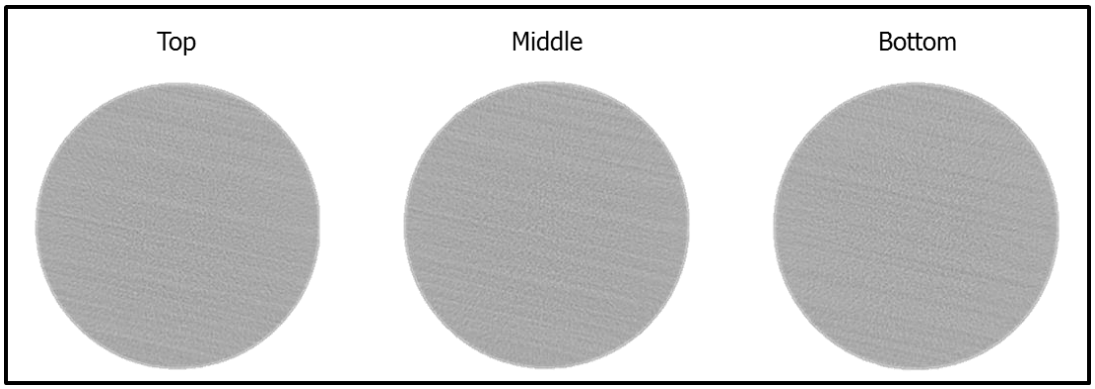

Figure 8. CT images of Berea Core # 2

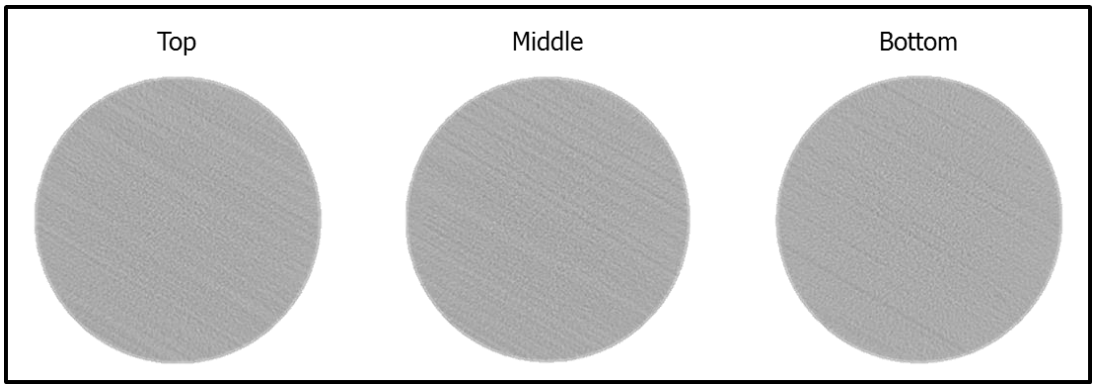

Figure 9. CT images of Berea Core # 3

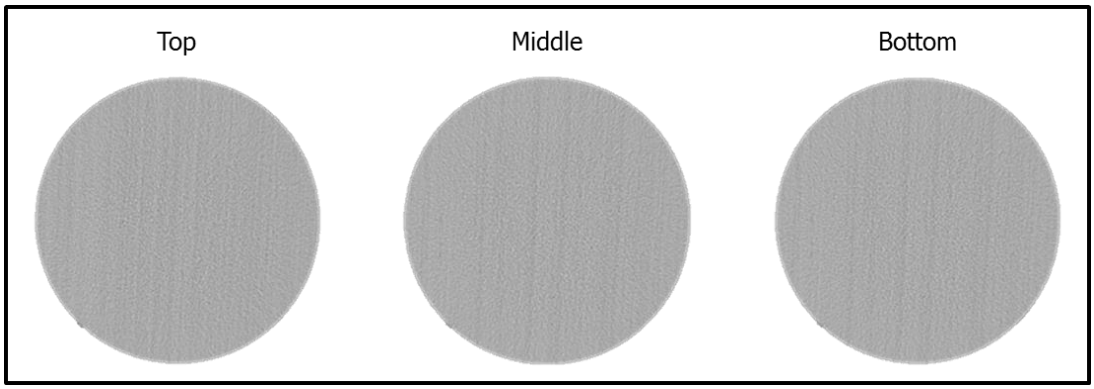

Figure 10. CT images of Berea Core # 4

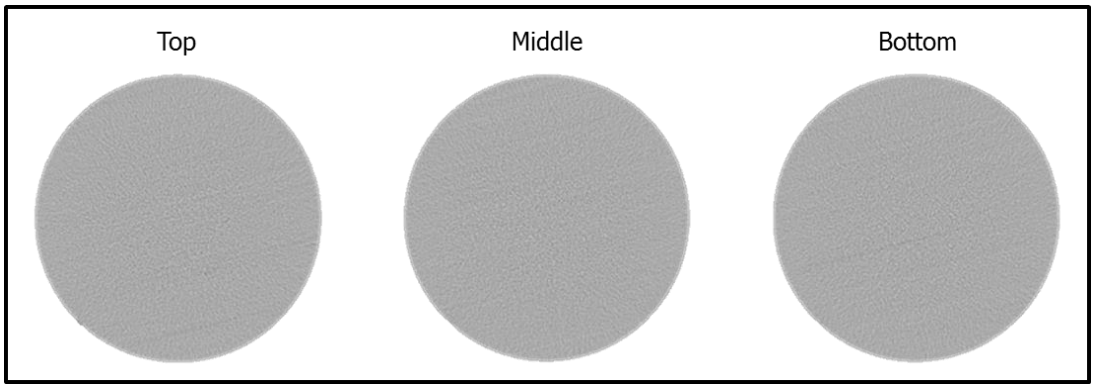

Figure 11. CT images of Berea Core # 5

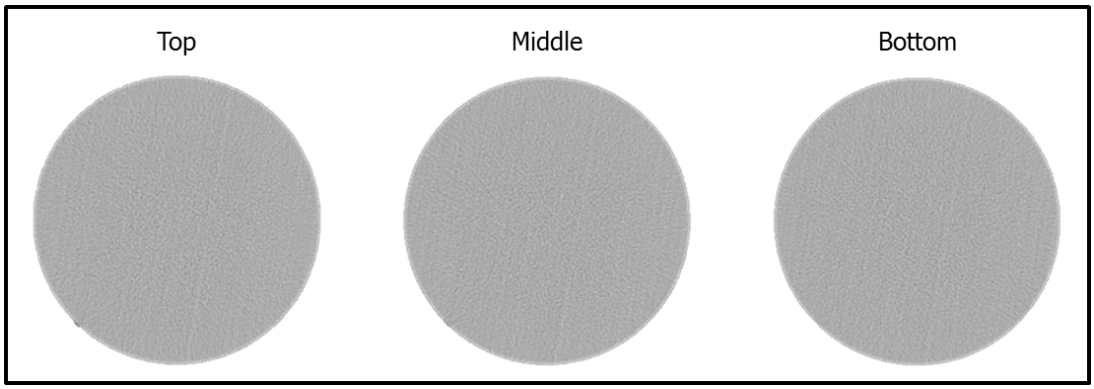

Figure 12. CT images of Berea Core # 6

IV.1.2 Rock Samples Experiment 2

One single piece of Edwards limestone was used for experiment # 2. The diameter and height of the sample were 101.6[mm] and 508[mm] respectively. This sample was cut from an Edwards limestone outcrop close to Carton Creek in Austin, Texas. Vuggy porosity can be easily identified at the surface of the sample (Figure 13). A detailed description of rock properties in this type of rock can be found at Izgec and Hill (2010). CT images were collected at different positions along the rock sample confirm a high presence of vugs (Figure 14).

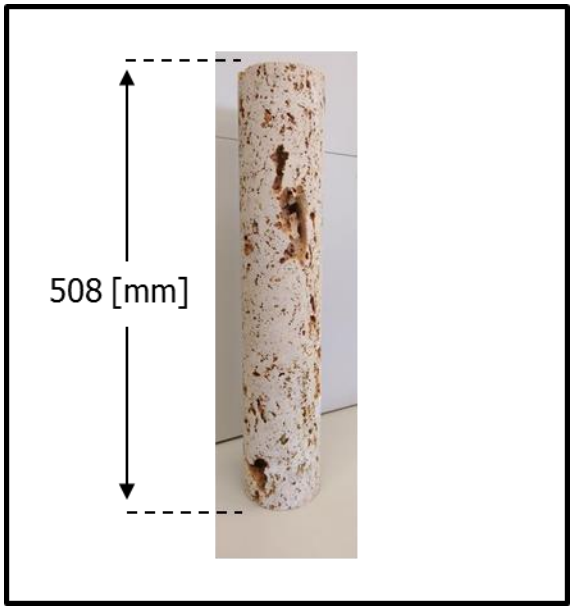

Figure 13. Edwards limestone core

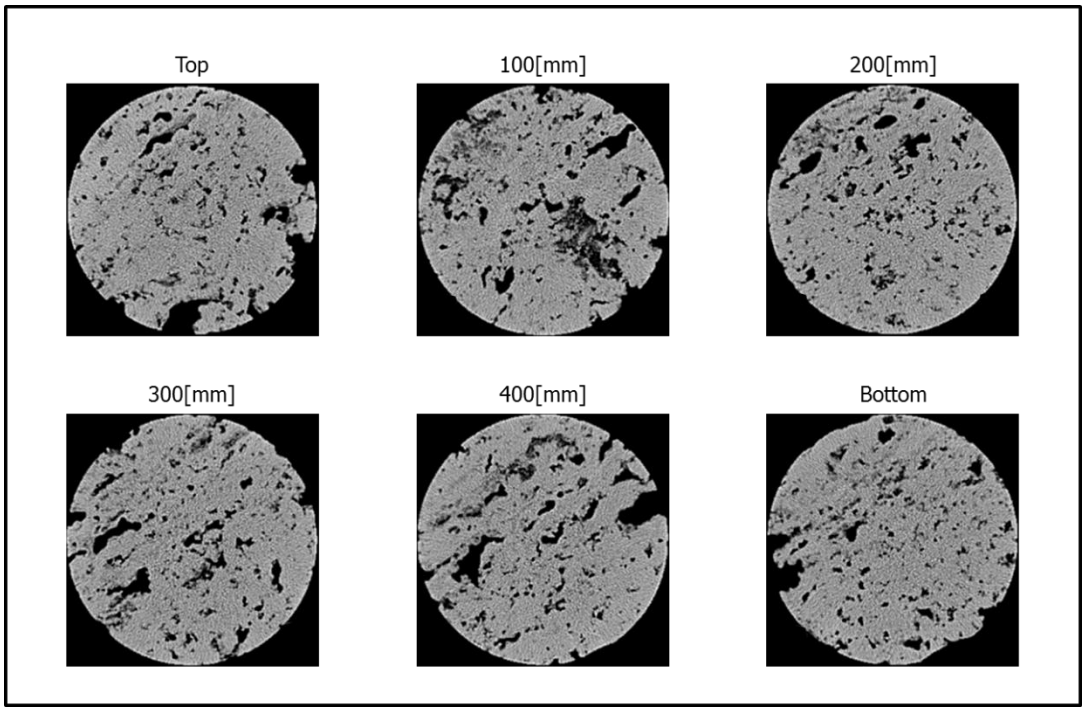

Figure 14. CT images of Edwards limestone core

IV.1.3 Fluids

For both experiments, the oil phase is the same. Because one of the parameters that define the velocity of the displacement is the viscosity, a low-density low-viscosity oil was selected.

For the experiment # 1, a brine solution was prepared using deionized water and 7wt% of sodium chloride (NaCl). There have been studies where it was observed that permeability of Berea sandstone decreases significantly if fresh water is injected into it (Mohan et al. 1993).

Table 1 shows the density and viscosity of both fluids at laboratory conditions:

Table 1. Oil and brine properties at 70[°F] and 14.7[psia]

Phase	Density[gr/cc]	Viscosity[cP]
Oil	0.72	1.06
Brine	1.05	0.97

The experiments were executed at controlled conditions; however laboratory temperature varied ± 2[°F] during the experiments. Fluid properties were measured at different temperatures and constant pressure (14.7[psia]) to assess the impact of those variations. Brine viscosity was computed according to the relations presented by McCain (1990). The observed variation in properties are insignificant hence, they can be assumed constant during the tests (Figure 15 to Figure 18).

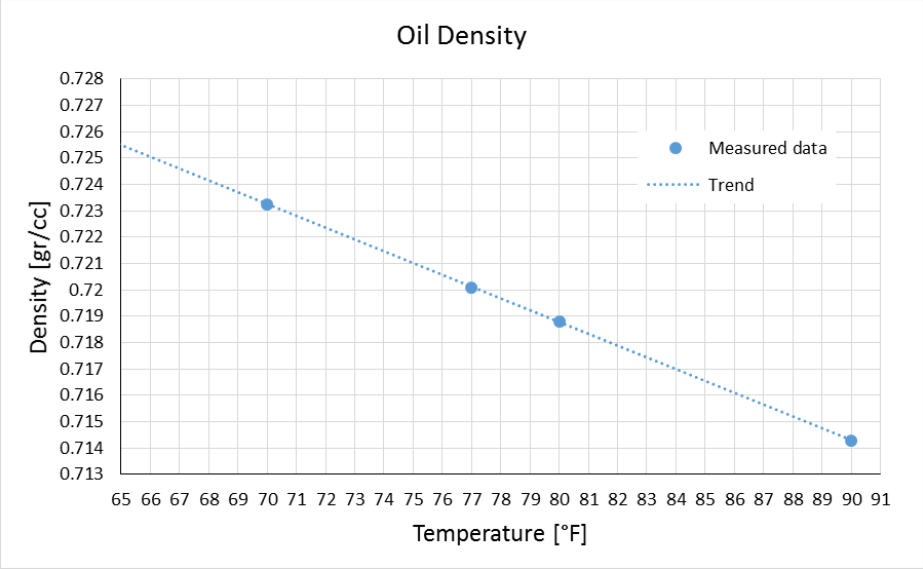

Figure 15. Oil density at 14.7[psia]

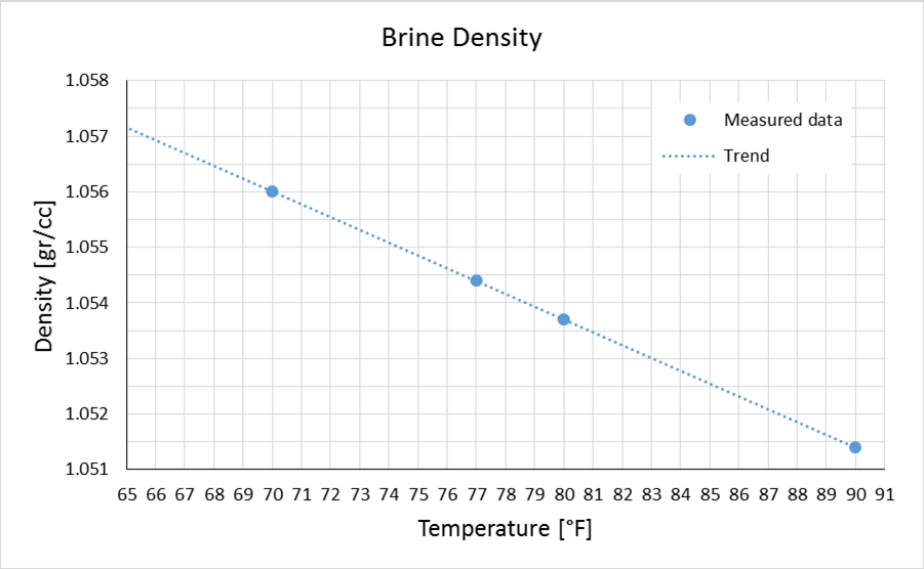

Figure 16. Brine density at 14.7[psia]

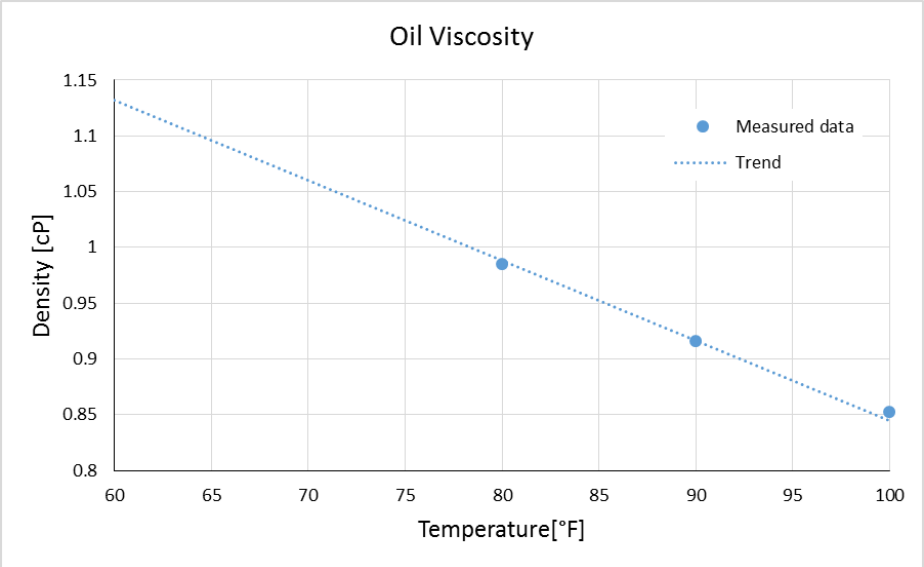

Figure 17. Oil viscosity at 14.7[psia]

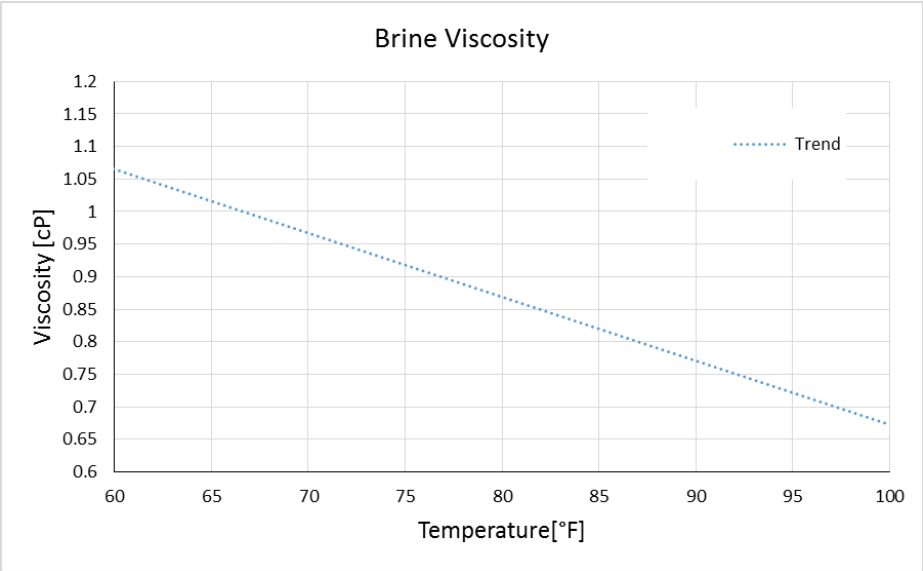

Figure 18. Brine viscosity at 14.7[psia]

IV.2 Experiment 1: Dual-Porosity Three-Phase Gravity Drainage

IV.2.1 Characterization of the Porosity

The six Berea rock samples were weighted at their dry condition. Then, they were piled up into the gravity drainage cell and CT images were taken over the stack (i.e. average CT_{ar} for the ROI was obtained from every CT slice captured along the stack). The data obtained from these CT images will be used for porosity determination as will be discussed later.

Once the CT images were taken over the stack at dry condition, Berea cores were taken out from the gravity drainage cell with the purpose of flood each single core with brine. A schematics of the apparatus used to flood the cores is shown in Figure 19.

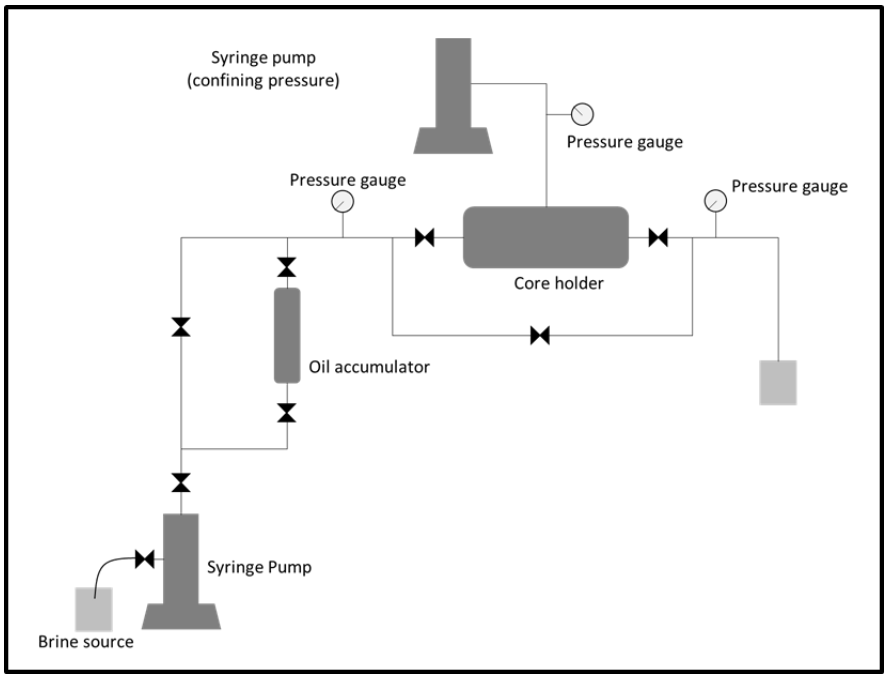

Figure 19. Schematics of apparatus used to flood Berea cores

A single Berea core was confined inside the core holder with a Viton sleeve. The confinement pressure was set up at 400[psia]. Once the core was confined, a syringe pump injected brine into the core. Valves that connect the oil accumulator to the flooding system were kept closed. After the core sample had been flooded and fully saturated with brine, it was removed from the core holder, weighted and placed into de gravity drainage cell surrounded by brine. This process was executed for all six Berea cores. When all the samples were piled up and surrounded by brine into the gravity drainage cell, a CT scans were taken over the stack. In this step, the average CT_{wr} for the ROI was obtained from every CT slice captured along the stack.

A first estimation of porosity for each Berea core was obtained by the relationship between its pore volume (V_p) and its bulk volume (V_b) defined as follows:

$$\phi = \frac{V_p}{V_b} \tag{4.1}$$

V_p is found by:

$$V_p = \frac{m_{wet} - m_{dry}}{\rho_w} \tag{4.2}$$

where m_{wet} is the weight of the core fully-saturated with brine, m_{dry} is the weight of the core at its dry condition and ρ_w is the brine density.

V_b is found by the computation of the volume occupied by a cylinder:

$$V_b = \pi\left(\frac{d}{2}\right)^2 h \tag{4.3}$$

where d and h are the diameter and the height of the core respectively.

Table 2 shows a summary of the weights obtained for each Berea core and their correspondent porosity according to Eqs. 4.1, 4.2., and 4.3.

Table 2. Berea sandstone porosity estimation based on weights

Sample	Dry weight [g]	Wet weight [g]	Porosity [%]
Core 1	2559.8	2804.0	18.5
Core 2	2638.9	2835.3	14.9
Core 3	2645.4	2836.0	14.5
Core 4	2579.4	2807.3	17.3
Core 5	2578.7	2813.3	17.8
Core 6	2634.5	2836.6	15.3

An additional computation of porosity was performed based on CT numbers obtained in the previous steps. The average CT number of the ROI (i.e. the region of the CT image that enclosed the core) for each slide was obtained from the CT scans along the cores at their dry and fully saturated with brine conditions. The software ImageJ was used to visualize CT images and to get the average CT number of the ROI in each slide. Then, by applying Eq. 3.6, a porosity distribution is obtained along the stack (Figure 20).

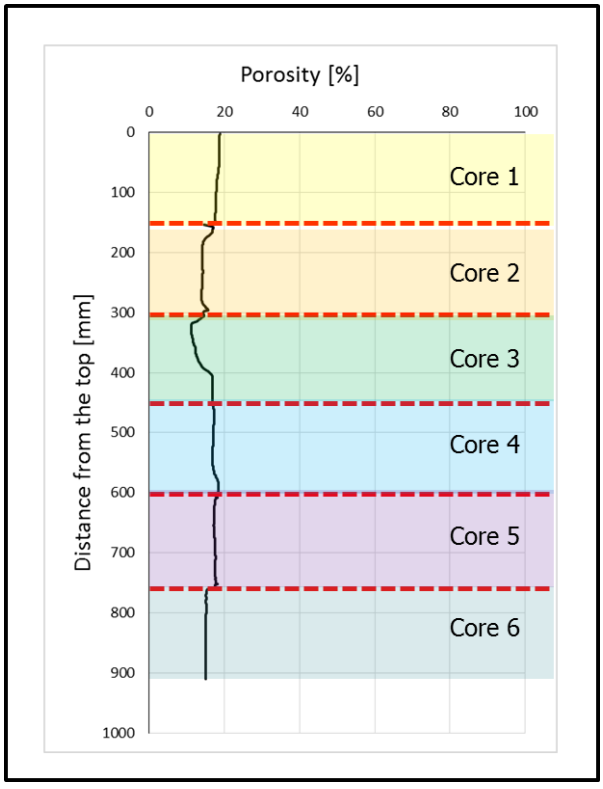

Figure 20. Porosity estimation of Berea samples based on CT values

Table 3 shows a comparison between the porosity estimated from weights and the average porosity obtained from CT data for each Berea rock sample.

Considering the data showed in Table 3, we can observe that there is a good agreement between the two methods.

Table 3. Porosity comparison

Sample	Porosity by weights [%]	Porosity by CT numbers [%]
Core 1	18.5	18.2
Core 2	14.9	14.6
Core 3	14.5	14.1
Core 4	17.3	17.4
Core 5	17.8	17.5
Core 6	15.3	15.1

IV.2.2 Initial Conditions and Execution of Gravity Drainage Experiment

By using the same apparatus described in Figure 19, every single Berea core was flooded by injecting oil until irreducible water saturation was reached. Then, were piled up one by one into the gravity cell surrounded by oil. CT images were collected over the stack at this condition (i.e. average CT_{aor} for the ROI was obtained from every CT slice captured along the stack). Since the only two phases were present in the rock samples, oil

saturations were computed by using Eq. 3.8 and Eq. 3.11. Figure 21 shows the initial oil saturation along the stack.

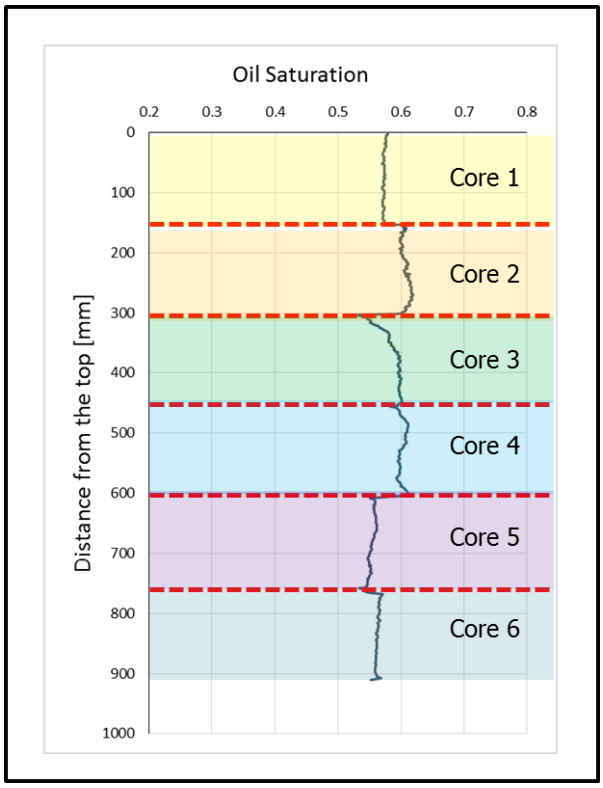

Figure 21. Initial oil saturation in Berea samples based on CT values

Table 4 shows the average irreducible water saturation, oil saturation and initial oil volume for each Berea core. The total oil volume contained into the stack was 694[cc].

Table 4. Initial oil saturation and initial oil volume Experiment 1

Sample	S_w [fraction]	S_o [fraction]	Oil volume [cc]
Core 1	0.43	0.57	129
Core 2	0.39	0.61	110
Core 3	0.41	0.59	103
Core 4	0.4	0.60	129
Core 5	0.45	0.55	119
Core 6	0.44	0.56	104
		Total	694

The volume of oil surrounding the stack was 3638[cc]. This volume was consi**d**ered as the fracture oil volume. Then gravity drainage cell is closed, and the valves at the top and bottom are opened simultaneously. At this moment, oil started flowing by gravity at the bottom. Air from the top port replaced the drained oil. Oil produced was tracked by the balance during the experiment.

Figure 22 shows the cumulative oil produced during the period (18400[min]) that experiment was performed. It is easy to see that there is a huge increment of produced oil in a very short period compared to the duration of the experiment. This rapid production represents the oil recovered from the fracture (defined by the gap between the interior of the cell and the stack). No water production was observed during the experiment.

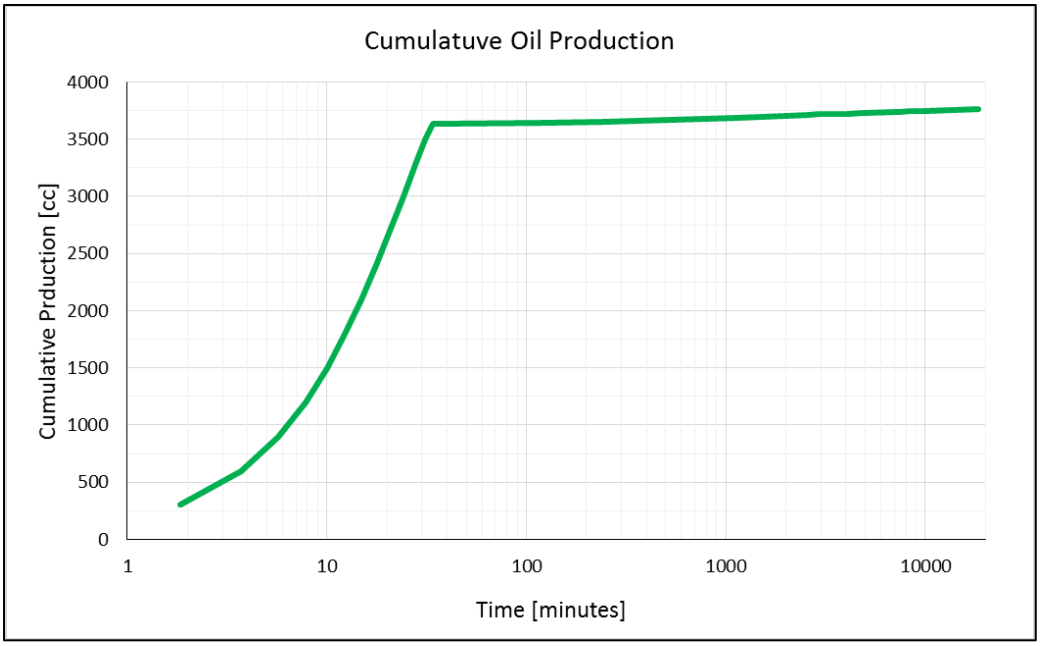

Figure 22. Total cumulative oil production in experiment 1

Excluding this period of rapid production, it is possible to see a smoothed behavior of the oil production for the rest of the experiment (Figure 23). Once the fracture was drained, it is assumed that all the oil produced from this point is attributed to the oil recovered by gravity drainage from the matrix. Figure 24 shows the oil recovery factor from the stack after fracture does not contribute to the oil production anymore.

IV.2.3 Volumetric Performance based on CT Images

During this period of gravity drainage, four CT scans were performed in order to track the distribution of fluids along the stack (Figure 25).

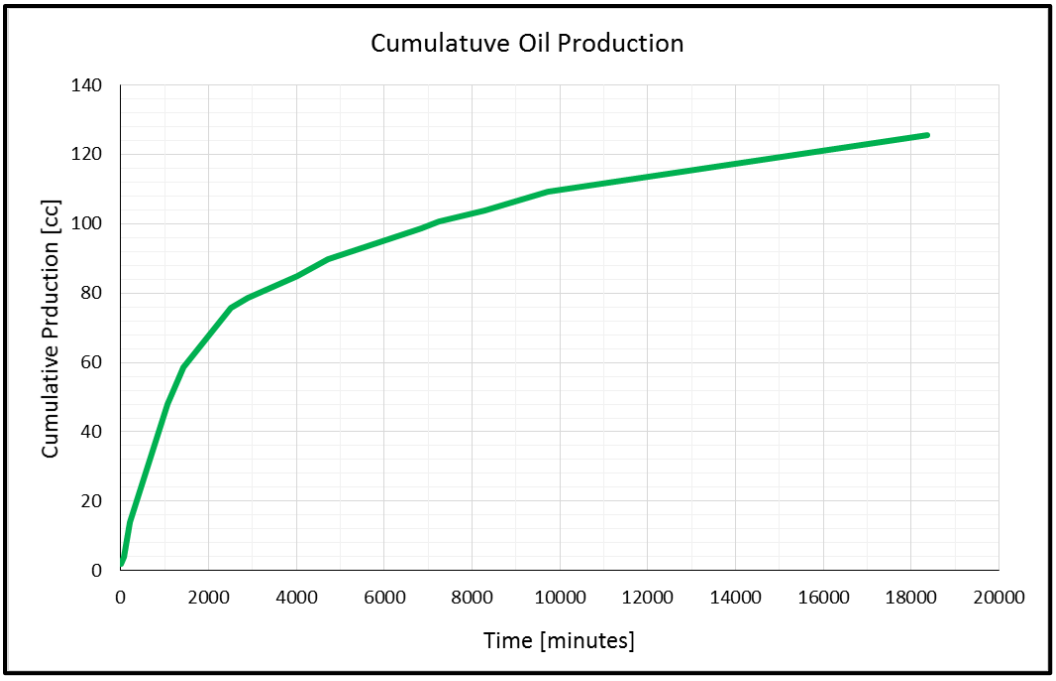

Figure 23. Cumulative oil production experiment 1 (after fracture was emptied)

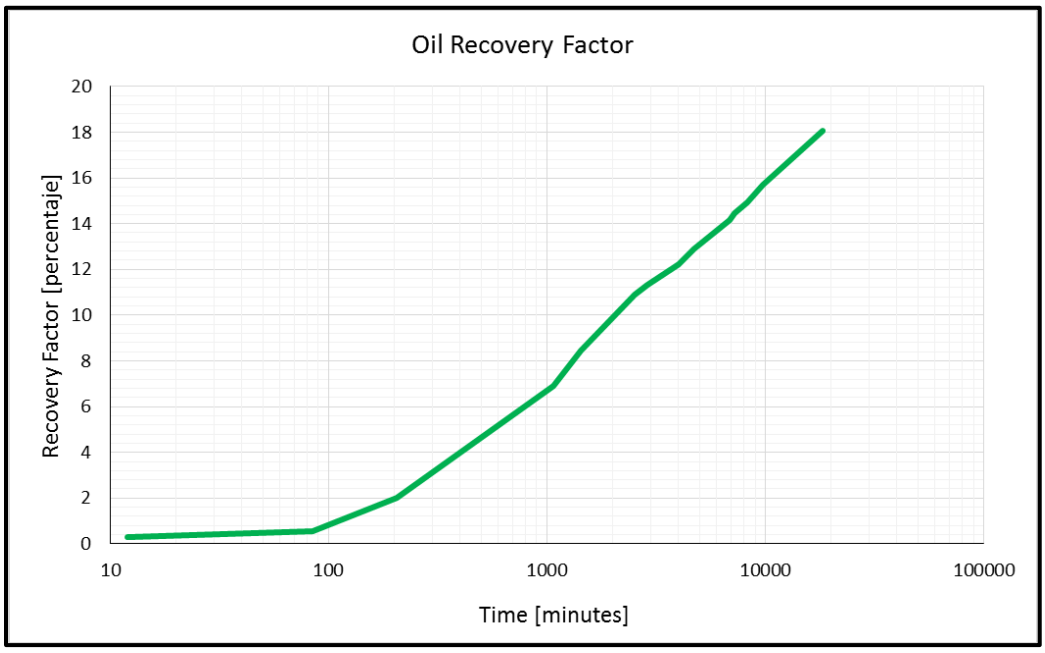

Figure 24. Oil recovery factor experiment 1 (after fracture was emptied)

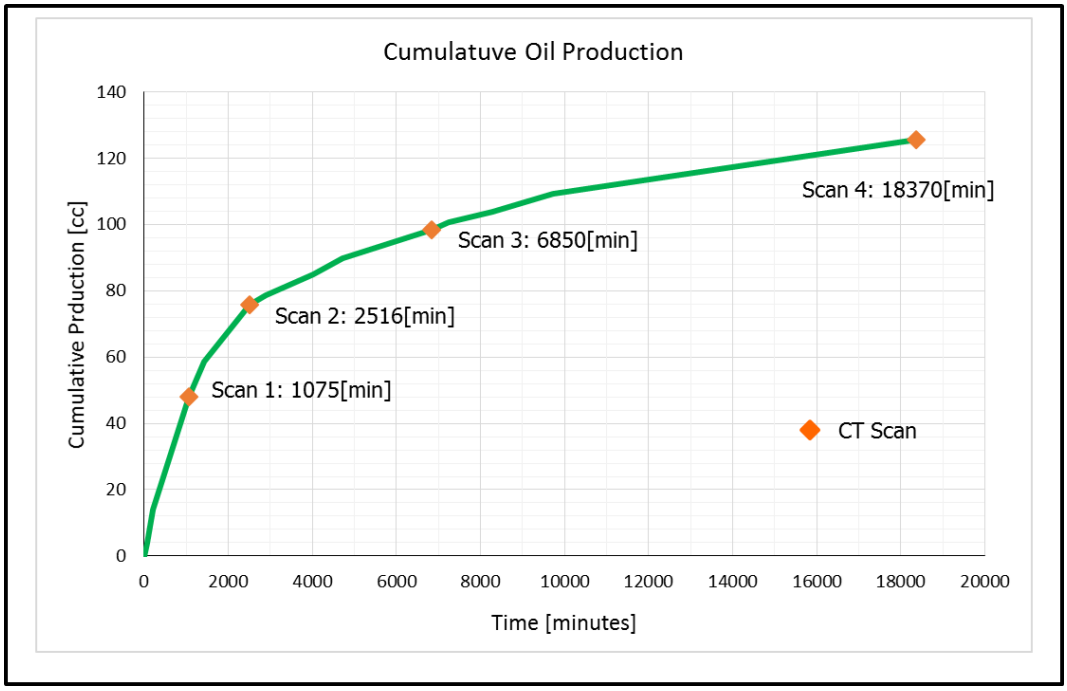

Figure 25. Time lapse CT scans in experiment 1 (after fracture was emptied)

Given that the irreducible water saturation was known at the initial condition for every single core, and considering the fact that none water production was observed during the experiment, the oil saturation distribution along the stack was computed by the method of immobile phase defined by MacAllister et al. (1993) using the CT data collected in each slice along the stack:

$$S_o = \frac{CT_{ar} - \left[CT_{awor} - S_{wi}\left(CT_{wr} - CT_{ar}\right)\right]}{CT_{ar} - CT_{or}} \tag{4.4}$$

where CT_{awor} is the CT number at the time scans were taken during the experiment, and S_{wi} is the irreducible water saturation already computed at the initial conditions. Note that CT values used in Eq. 4.4 are the average values obtained for the region of interest in each CT slide.

Figure 26 shows the oil saturation distribution along the stack obtained from the CT images.

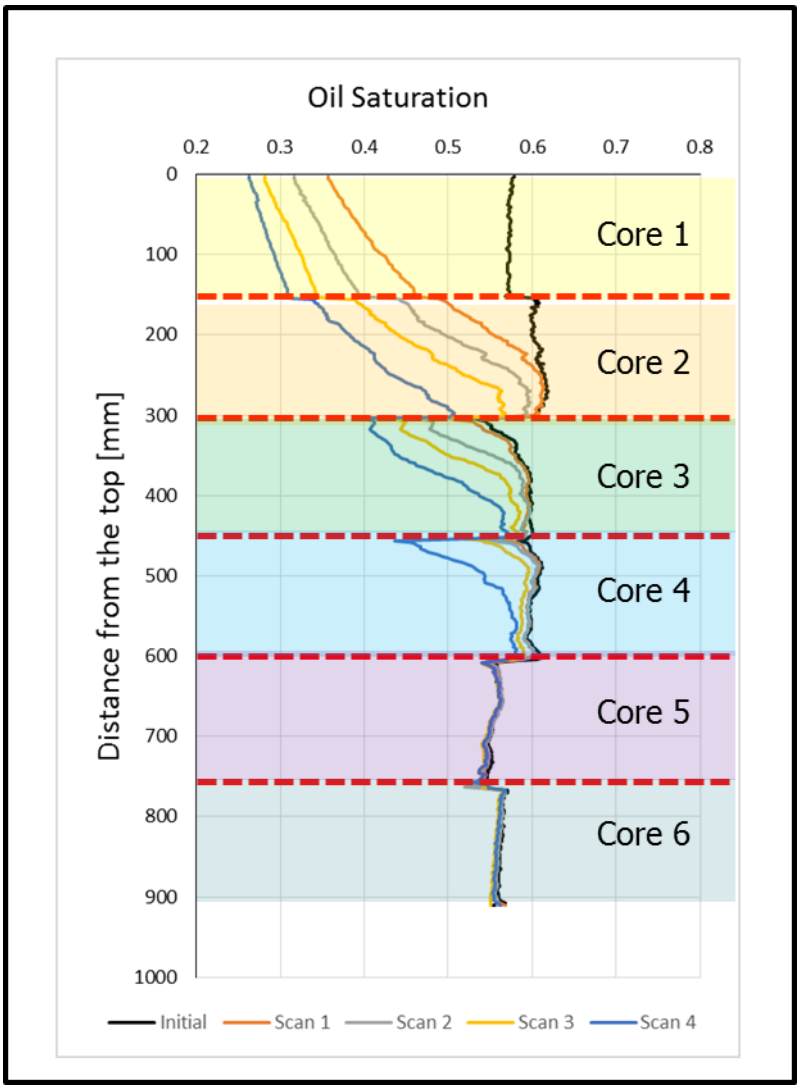

Figure 26. Changes in oil saturations along the stack in experiment 1

Table 5 and Table 6 shows the average oil saturation and the oil volume in matrix respectively for each core at the times CT images were collected.

Table 5. Average oil saturation during experiment 1

Sample	S_o Initial (frac)	S_o Scan 1 (frac)	S_o Scan 2 (frac)	S_o Scan 3 (frac)	S_o Scan 4 (frac)
Core 1	0.57	0.41	0.35	0.31	0.29
Core 2	0.61	0.57	0.53	0.48	0.42
Core 3	0.59	0.58	0.56	0.53	0.49
Core 4	0.60	0.60	0.59	0.58	0.55
Core 5	0.55	0.55	0.55	0.55	0.55
Core 6	0.56	0.56	0.56	0.56	0.56

Table 6. Oil volume in matrix during experiment 1

Sample	Initial (cc)	Scan 1 (cc)	Scan 2 (cc)	Scan 3 (cc)	Scan 4 (cc)
Core 1	129	91	80	70	64
Core 2	110	104	96	87	75
Core 3	103	102	98	94	86
Core 4	129	128	128	125	118
Core 5	119	119	119	119	119
Core 6	104	104	104	104	104
Total	694	648	625	599	566

In order to compare the oil volumes obtained by the CT scans and the cumulative oil produced at time they were taken, a volumetric balance is performed:

The cumulative oil produced from matrix estimated from CT scan data is computed as follows:

$$Np_{CT} = Vo_i - Vo_{CT} \tag{4.5}$$

where Np_{CT} is the cumulative oil produced from the matrix estimated by CT data for the stack, Vo_i is the initial oil volume obtained by CT data for the stack, Vo_{CT} is the oil volume obtained from CT data at the time scans were collected during the experiment.

The cumulative oil produced from matrix estimated from registered volumes at the time CT scans were taken:

$$Np_{vol} = Np - Vof \tag{4.6}$$

where Np_{vol} is cumulative oil produced from the matrix, Np is the total cumulative oil produced at the time CT scan were performed, and Vo_f is the oil volume contained in the fracture.

Table 7 shows a comparison of the oil volumes recovered from the matrix by the two balances. Note that the produced oil volumes obtained by the CT scans match very closely the production tracked during the experiment.

Table 7. Comparison of oil recovered from matrix during experiment 1

	Np_{CT} (cc)	Np_{vol} (cc)
Scan 1	46	48
Scan 2	69	76
Scan 3	95	98
Scan 4	128	126

IV.3 Experiment 2: Triple-Porosity Two-Phase Gravity Drainage

IV.3.1 Characterization of the Porosity

As it was shown in the Figure 14, rock sample used in this experiment reveals a high heterogeneity due to the presence of vugs. A simple computation of average porosity considering the two systems (matrix and vugs) may not be adequate to determine changes in oil saturation along the core during the gravity drainage experiments. On the other hand, at the time the experiment begins, oil contained in vugs that are in touch with the fracture (i.e. touching vugs) and oil contained in the fracture (Figure 27) would be drained at the same time. Considering the previous situation, a splitting of the pore system along the cores is necessary to evaluate the performance of gravity drainage in this experiment.

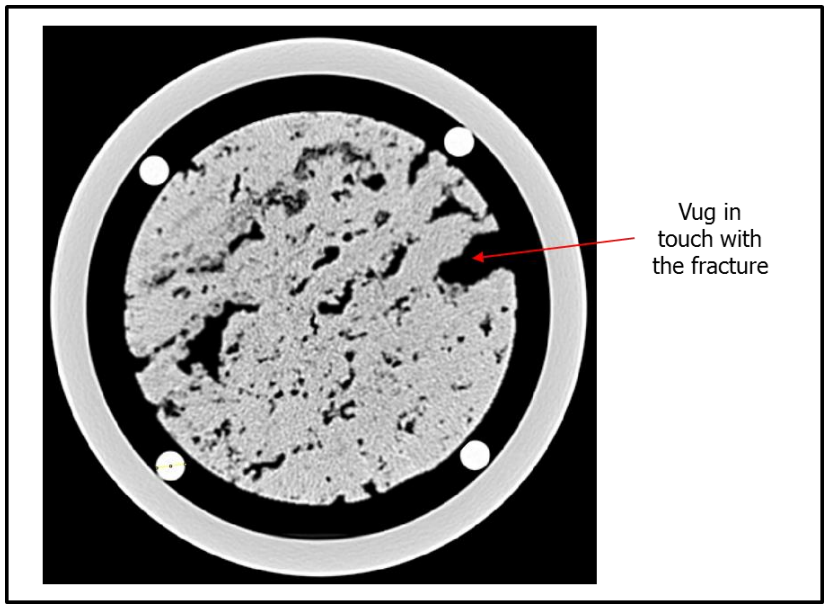

Figure 27. CT image of Edwards limestone into the gravity drainage cell

In order to identify and quantify porosities for the matrix, the touching vugs, and the non-touching vugs (e.g. vugs that are not in touch with the fracture) a workflow was designed (Figure 28).

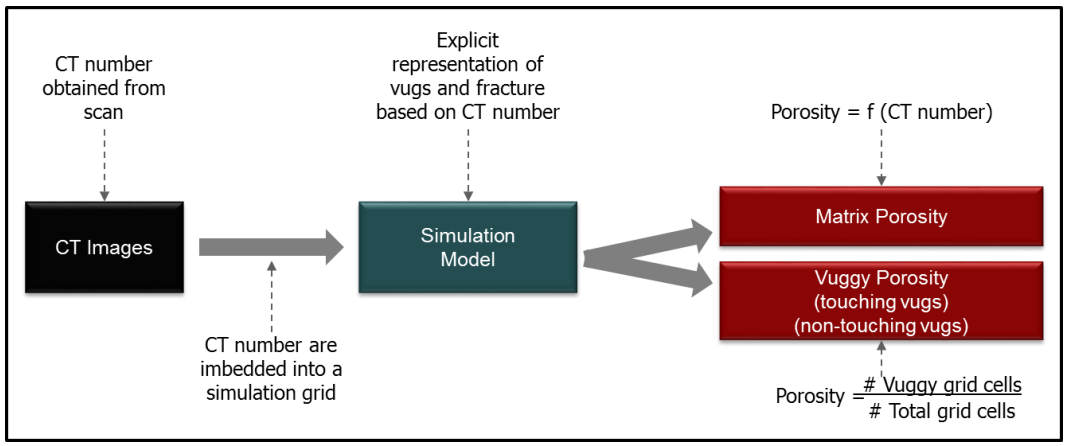

Figure 28. Workflow designed to quantify porosity for each porous system in experiment 2

In this workflow, the CT values obtained from each slice are exported and then embedded into a simulation grid. Since the CT images contain 512 x 512 voxels in each slice, and every CT image was collected with a resolution of 1[mm] along the core resulting in a total of 508 slices, the simulation grid was constructed with a size of 512 x 512 x 508. Once the simulation grid contains the CT number, a binarization is performed: simulation grid cells with low CT are labeled as vuggy cells; simulation grid cells with high CT values are labeled as matrix cells. For those cells identified as vuggy cells, high values of porosity and permeability are assigned (e.g. porosity = 100% and permeability = 1[D]). For those matrix cells, arbitrary values of porosity and permeability are assigned. After properties have been allocated to each cell, the simulation grid is initialized with a single fluid. Then, matrix cells are deactivated in the simulation grid leaving active only the vuggy cells. Finally, a simulation of a fluid injection in a closed system is performed; during the simulation, the fluid is injected through the cells that represent the fracture. At

the end of the simulation, vugs that exhibit a change in pressure are considered touching vugs; vugs that kept the same pressure during the simulation are considered non-touching vugs. Figure 29 shows a schematic of the simulation process described.

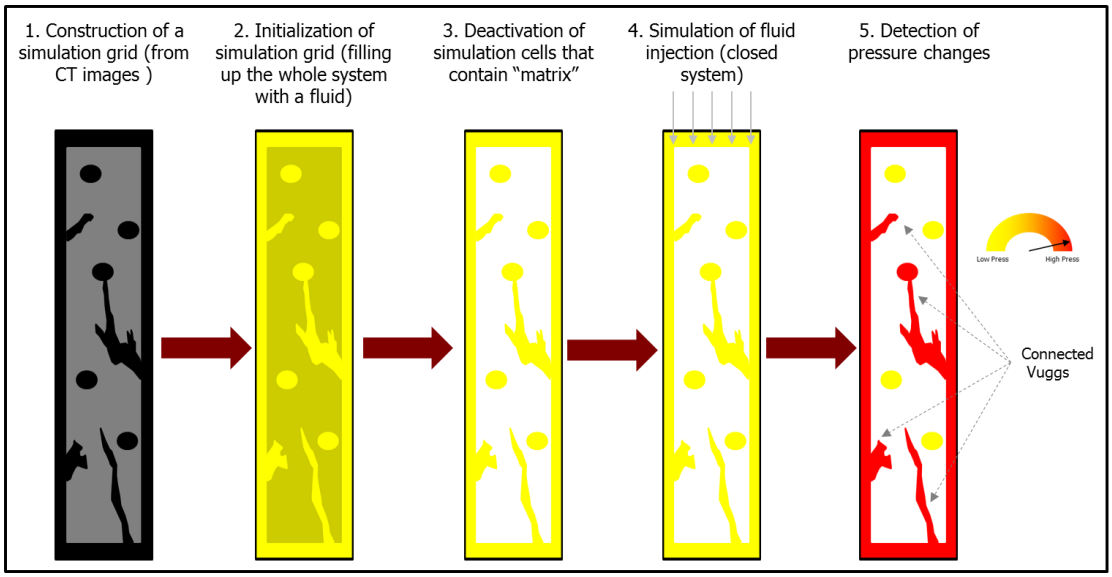

Figure 29. Detection of touching vugs

An example of the final splitting of the porous system is shown in Figure 30. Left image shows the CT image embedded into a simulation grid. Right image shows the partition of the porous system after the execution of the workflow.

In the right side of Figure 30, the region of interest (ROI) is enclosed by the white circle. The dark blue region represents the fracture in the simulation model; this region is synthetic and does not represent the real gap between the gravity drainage cell and the core. The light blue region represents the vugs that are in touch to the fracture. This region

shows vugs that are directly in contact with the fracture. However, there are some vugs that appear to be surrounded by matrix; these apparent matrix-surrounded vugs are in contact with adjacent or subjacent vugs that at the same time are in touch to the fracture. The yellow region represents the non-touching vugs, and the orange region represents the matrix.

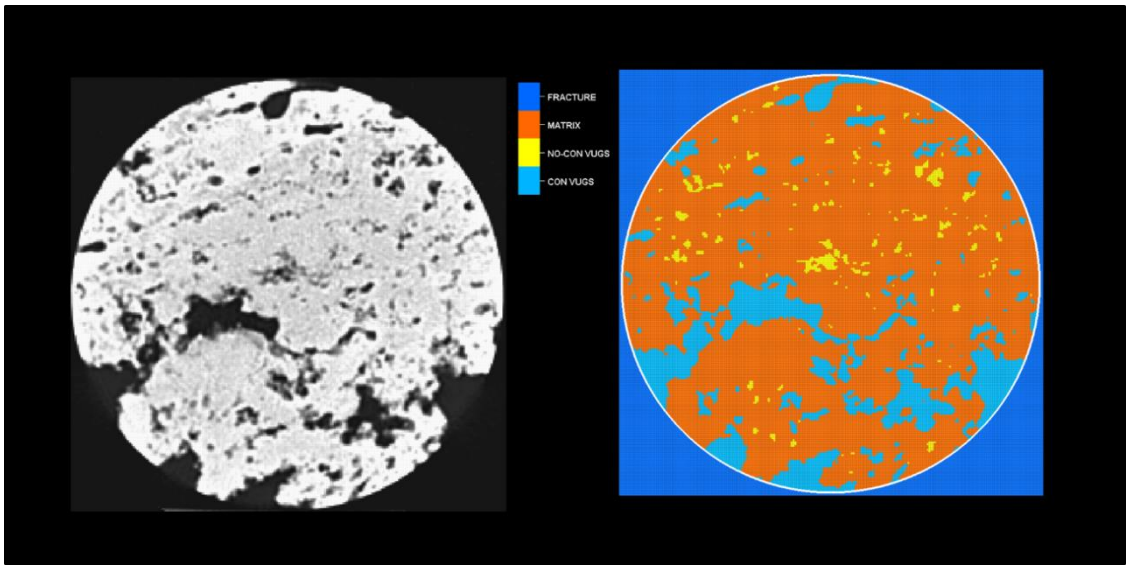

Figure 30. Separation of porous system experiment 2.

For this experiment, porosity is estimated for each system separately: for every single layer into the simulation grid, matrix porosity was computed as it was defined in Eq. (3.6):

$$\phi_m = \frac{CT_{ar} - CT_{or}}{CT_a - CT_o} \tag{4.5}$$

where the subscripts *ar* and *or* denote the CT number of the matrix saturated with air and the matrix saturated with oil respectively; the subscripts *a* and *o* denote the CT number of the air and oil respectively. Note that the values CT_{ar} and CT_{or} in Eq. 4.5 are the average values for those cell identified as matrix cells contained in each layer into the simulation grid.

In a similar manner, touching vuggy porosity was estimated for each layer by:

$$\phi_{cv} = \frac{TNCV}{TROI} \tag{4.6}$$

where TNCV represents the total number of cells contained in the region of interest in the simulation layer identified as touching vugs, and TROI represents the total number of cells contained in the region of interest (ROI) for the same layer.

Non-touching vuggy porosity:

$$\phi_{iv} = \frac{TNIV}{TROI} \tag{4.7}$$

where TNIV represents the total number of cells contained in the region identified as non-touching vugs.

In a similar way to experiment 1, Edwards sample was scanned at its dry condition (saturated with air). Then, the core sample was placed into the gravity drainage cell full of oil. By cycles of vacuuming and pumping, the sample was saturated 100% with oil. Core sample filled with oil was scanned again.

Using the workflow described to split the system, and computing the porosity using the Eq. 4.5 to Eq. 4.7, the distribution of porosities along the core was obtained.

Figure 31 shows the results obtained. From this figure, gray line in the plot represents the porosity distribution of the non-touching vugs; orange line represents the total porosity due to the presence of vugs (touching vugs + non-touching vugs); the blue line corresponds to the total porosity of the rock (touching vugs + non-touching vugs + matrix). Table 8 shows a summary of the porosities for each system.

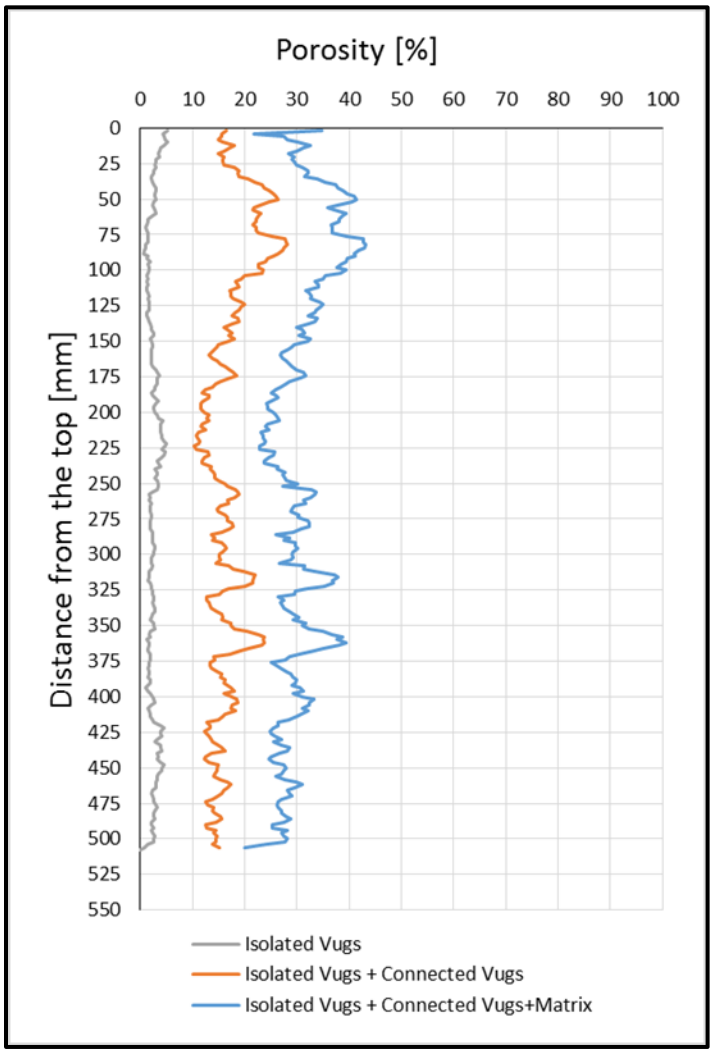

Figure 31. Porosity distribution along the rock sample in experiment 2

From Figure 31 it is possible to see that non-touching vugs have a poor contribution to the total porosity. On the other hand, matrix and touching vugs dominate the total porosity profile along the core. Additionally, we can observe that high connectivity caused by the touching vugs is present in the whole rock sample.

Table 8. Average distribution of porosity and pore volumes in Edwards rock sample

System	Porosity [%]	Pore Volume[cc]
Non-touching vugs	2.5	48.5
Touching vugs	14.3	275.8
Matrix	13.7	217.6

Note that pore volumes presented in Table 8 are equal to initial oil volumes in each system given that the rock sample is filled 100% with the oil.

IV.3.2 Initial Conditions and Execution of Gravity Drainage Experiment

With the core fully saturated (i.e. S_o = 1) and surrounded by oil into the closed gravity drainage cell, the top and bottom valves of were opened simultaneously. The volume of oil surrounding the stack is 6940[mm]. This volume is considered as the fracture oil volume. At this moment, oil started to flow at the bottom. Air coming into the cell from the top port replaced the drained oil. From this point, oil produced is tracked by the balance during the experiment.

Figure 32 shows the cumulative oil produced during the experiment was performed. In a similar manner than in experiment 1, there is a short period where a rapid production is observed. This rapid production is dominated by the oil drained from the fracture (defined by the gap between the interior of the cell and the stack) and the touching vugs.

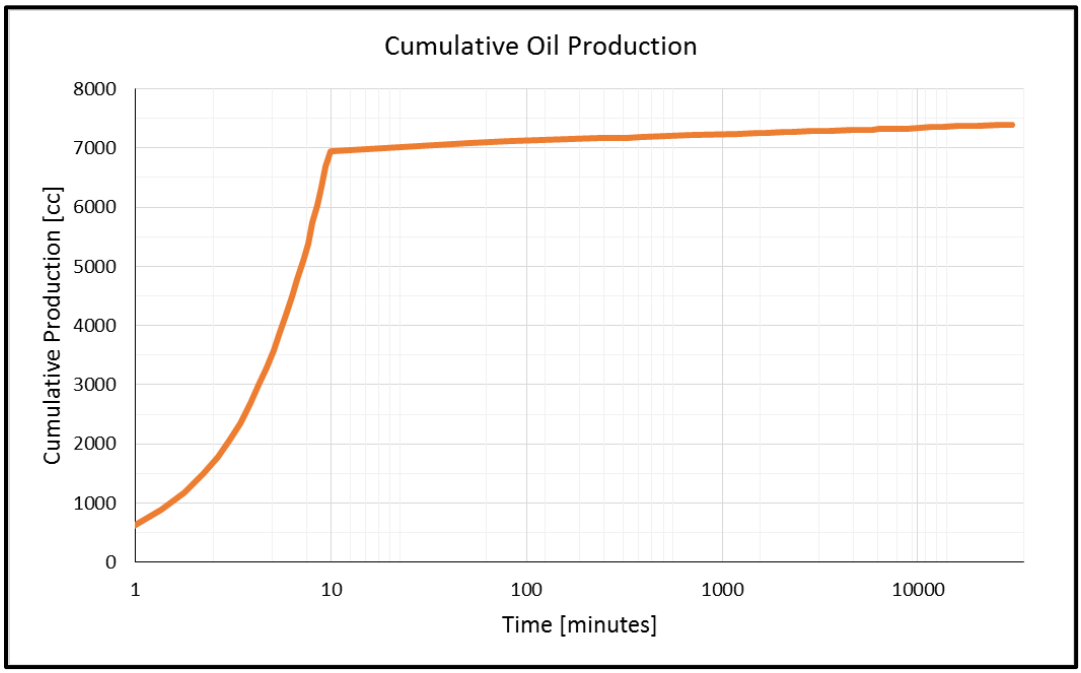

Figure 32. Total cumulative oil production experiment 2

Unlike the experiment 1, in experiment 2 is not possible to separate the oil produced from the fracture; oil from the fracture and oil from the touching vugs flow simultaneously downwards at the time the ports at the gravity drainage cells are opened. Figure 33 marks the time at which fracture volume was reached. As we can note, after

fracture volume has been reached, oil production still increasing rapidly till the total reaches approximately 7150[cc].

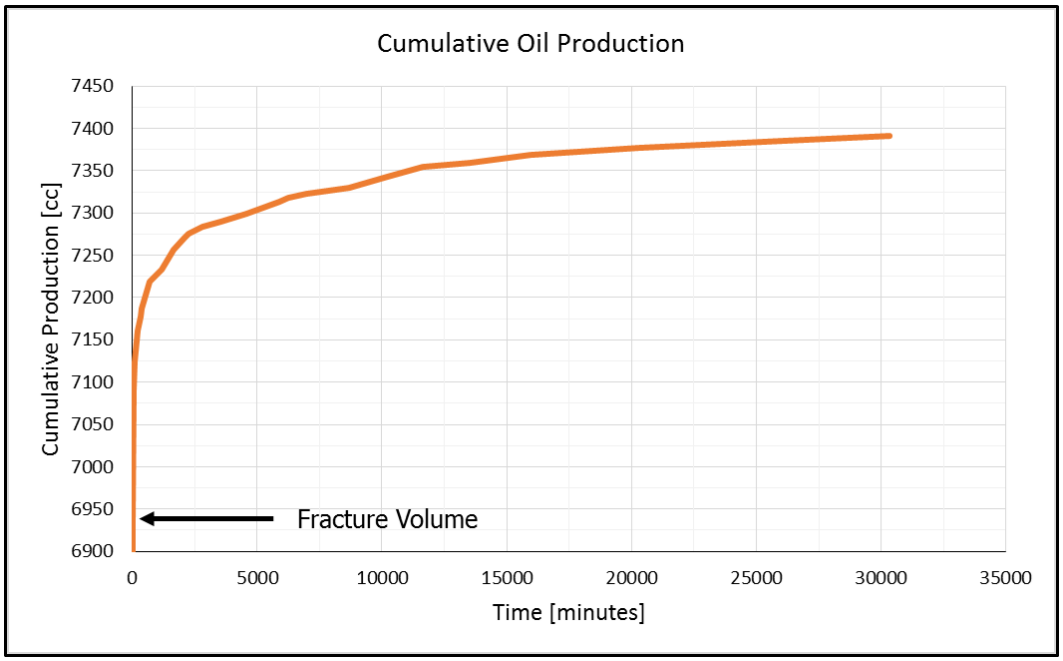

Figure 33. Total cumulative oil production experiment 2

IV.3.3 Volumetric Performance based on CT images

During the period of gravity drainage, six CT scans were performed in order to track the oil saturation in the matrix along the core (Figure 34).

In the same manner as in porosity determination for the rock used in this experiment, workflow designed to split the porous system is performed using the data collected from the CT scans at different times. By using the Eq. 3.8 for a system where

only air and oil are present, the oil saturation in matrix for each layer into the simulation grid was computed for the times where CT data was collected.

$$S_o = \frac{CT_{oar} - CT_{ar}}{CT_{or} - CT_{ar}} \tag{4.8}$$

where CT_{aor} is the average CT number of the matrix cells for each simulation layer at the time scans were taken during the experiment. Note that the mean values CT_{aor} and CT_{aor} for each simulation layer have been already computed for porosity determination.

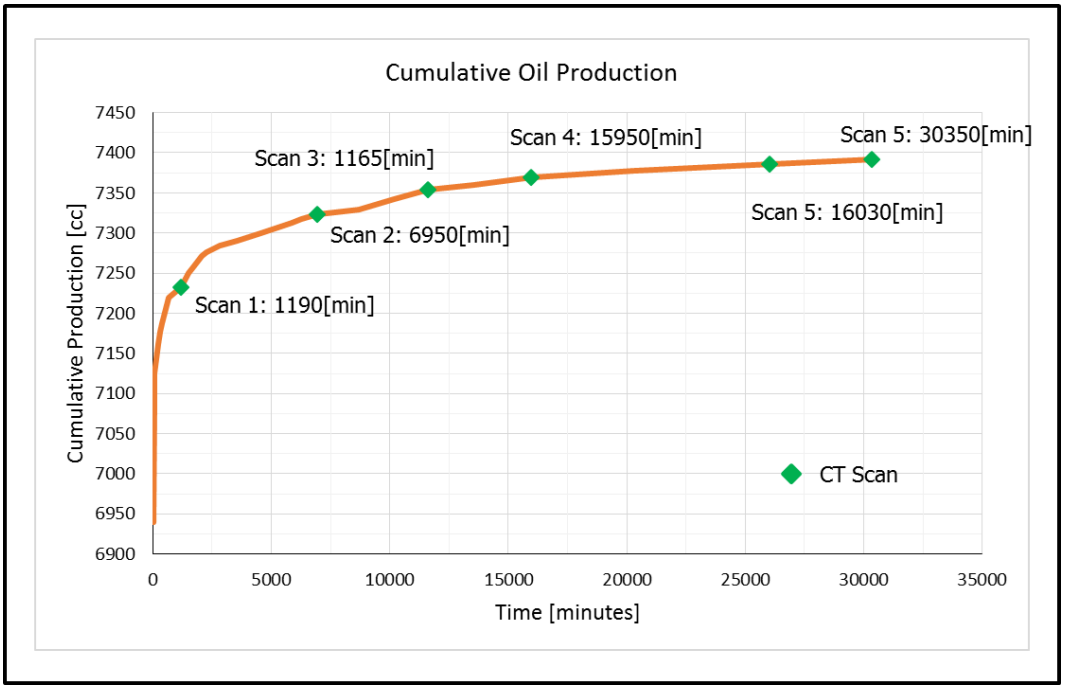

Figure 34. Cumulative oil production experiment 2 (after fracture and touching vugs were emptied).

Figure 35 shows the oil saturation distribution in the matrix along the stack obtained from the CT images.

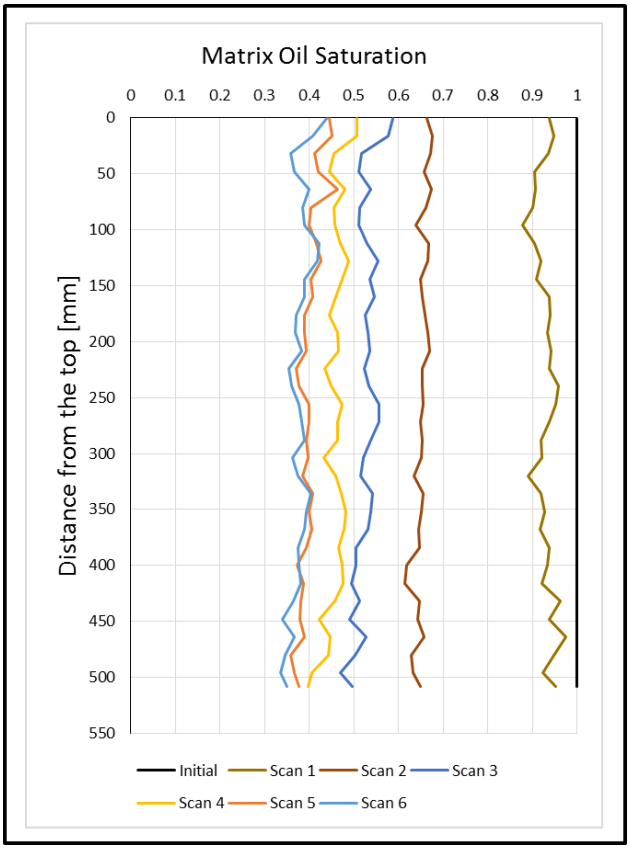

Figure 35. Changes in oil saturations in the matrix along the core in experiment 2

Table 9 shows an average oil saturation and the oil volume in the matrix at the times CT images were taken.

Table 9. Average oil saturation and oil volume in the matrix during experiment 2

	Oil Saturation [fraction]	Oil volume [cc]
Initial	1.00	217.7
Scan 1	0.93	202.1
Scan 2	0.65	141.9
Scan 3	0.52	114.4
Scan 4	0.46	100.1
Scan 5	0.40	86.8
Scan 6	0.38	82.4

Changes in oil volume and oil saturation for the non-touching vugs are approximated by a volumetric balance. It is assumed that oil contained in the touching vugs and the fracture have been totally drained at the time CT scans were taken. Then, the volume of the non-touching vugs is defined as follows:

$$Np_{ncv} = Np - Np_m - Vo_f - Vo_{cv} \tag{4.9}$$

$$Vo_{ncv} = Voi_{ncv} - Np_{ncv} \tag{4.10}$$

where Np_{ncv} is the cumulative oil produced recovered from the non-touching vugs, Np is the total cumulative oil produced at the time CT scan was taken, Np_m is the difference between the estimated oil volume in the matrix at the time CT scans were taken and the initial oil volume in the matrix, Vo_f is the oil contained in the fracture, Vo_{cv} is the initial oil volume contained in the touching vugs, Vo_{ncv} is the remaining oil volume in the non-touching vugs, and Voi_{ncv} is the initial oil volume in non-touching vugs.

The average oil saturation in the non-touching vugs was obtained by:

$$So_{ncv} = \frac{Vo_{ncv}}{Voi_{ncv}} \tag{4.11}$$

where So_{ncv} is the oil saturation in the non-touching vugs and

Table 10 shows the volume of oil and the oil saturation in the non-touching vugs at the time CT scans were performed.

Table 10. Average oil saturation and oil volume in the non-touching vugs during experiment 2

	Oil volume [cc]	**Oil saturation [fraction]**
Scan 2	47.06	0.97
Scan 3	17.35	0.36
Scan 4	13.29	0.27
Scan 5	13.12	0.27
Scan 6	9.62	0.20

CHAPTER V

CONCLUSIONS AND RECOMMENDATIONS

V.1 Summary and Conclusions

In the present thesis work two experiments that mimicked gravity drainage were performed. In experiment 1, a stack of Berea sandstone rock with 101.6[mm] and 914.44[mm] of radius and height respectively was used. Due to the single porosity present in the Berea samples, a fractured reservoir was emulated. In experiment 2, a one-piece of Edwards limestone with 101.6[mm] and 508[mm] of radius and height respectively was used. Since the presence of vuggy porosity in this sample, a fractured reservoir with the presence of secondary porosity was represented. X-Ray CT Images were used to characterize the porous system and to track the distribution of fluids during the experiments. With the results obtained during the study and the use of CT images, conclusions can be summarized for each experiment.

V.1.1 Experiment 1

1. Estimation of porosity for the six Berea cores was performed with two different methods: by using the measured weights of the cores at dry condition and fully saturated with brine; and using the CT number obtained from CT scans at the mentioned conditions. A good agreement between the two methods was found with a maximum difference 0.3%. Average porosities obtained from CT images were

18.%, 14.6%, 14.1%, 17.4%, 17.5% and 15.1% for the cores 1, 2, 3, 4, 5 and 6 respectively.

2. Berea cores were flooded with oil until irreducible water saturation was reached. Based on CT Images, irreducible water saturations was computed: 0.43, 0.39, 0.41, 0.4, 0.45, and 0.44 for cores 1, 2, 3, 4, 5 and 6 respectively.
3. The initial volume of oil in the stack was 694[cc]. The total oil produced from the stack due to the effect of gravity drainage was 126[cc] that represents a recovery factor of 18%. None water production was observed.
4. During the execution of the experiment, it was possible to track the distribution of fluids along the stack based on CT scans at four different times. Due to the characteristic of immobility of the water phase, and considering the fact that none water production was observed during the test, the method immobile phase proposed by MacAllister et al. (1993) was effective to compute the oil saturation along the stack.
5. A comparison between the produced oil tracked and the remaining oil volumes obtained by CT scans along the stack was made. The produced oil volumes estimated by CT scans match very closely the oil production tracked during the experiment through the balance.
6. For the period that the experiment spanned, no changes in the oil saturation were observed for the two cores located in the lower part of the stack.
7. Despite the capillary contact that exists among the cores in the stack, it was possible to observe that there is not continuity in the oil saturation at the

neighboring faces. This shows that capillary pressures are not the same for each core in the stack.

8. The result of this experiment presents a characterization of the porous system and oil saturation profiles in the matrix at different times by using X-CT images. The data presented in this work can contribute to the modeling of gravity drainage in naturally fractured reservoirs when vuggy porosity is present.

V.1.2 Experiment 2

1. A novel workflow was developed with the objective to characterize the porous system in an Edwards limestone core that has a high presence of vuggy porosity. The workflow transforms the CT images taken from the core into a simulation grid. Then, a synthetic numerical simulation is performed to identify connectivity among vugs present inside the core and also connectivity of the vugs with the natural fracture emulated by the gap between the core and the interior of the gravity drainage cell.
2. As a result of the workflow developed for this study, a partition of the porous system was achieved. Quantification of matrix porosity, touching vuggy porosity and non-touching vuggy porosity along the core was possible to this workflow.
3. Estimated porosity for non-touching vugs, touching vugs, and matrix was 2.5%, 14.3%, and 17.7% respectively.

4. Based on the estimated porosities, the initial volume of for each system was computed: 48.5[cc], 275.8[cc], and 217.6[cc] for non-touching vugs, touching vugs, and matrix respectively.
5. During this experiments, oil saturation in the matrix was tracked based on CT images. Oil saturation profiles were obtained at six different times. At the end of the experiment, the average oil saturation was 0.38 that represents 82.4[cc] Thus, the oil recovery factor from matrix resulted as 62%. It was assumed that touching vugs were totally drained.
6. Assuming that oil volumes contained in the fracture and the touching vugs were totally drained at the time CT scans were taken, average saturation in non-touching vugs was estimated by a volumetric balance. The oil volume in the non-touching vugs at the end of the experiment was 9.62[cc] that represent an oil saturation of 0.2 therefore, a recovery factor of 80% was achieved.
7. Despite this experiment included a two-phase system, behavior of oil saturation profiles does not show smoothed changes. That suggest that capillary effects for the system oil-air used in this experiment are negligible.
8. The result of this experiment presents a characterization of the porous system and oil saturation profiles in the matrix at different times by using X-CT images. The data presented in this work can contribute to the modeling of gravity drainage in naturally fractured reservoirs when vuggy porosity is present.

V.2 Future Work and Recommendations

Compared to similar analysis where gas-oil gravity drainage in naturally fractured reservoir was studied, results from experiment 1 showed that the presence of water in the rock samples affects the velocity of the oil displaced by gravity drainage. Since the residual oil saturation was not achieved during the time that the experiment was performed, a way to approach an estimation of the final oil recovery factor and the time that may take to reach it is by constructing a simulation model that matches the oil production and oil saturation profiles obtained during the experiment. For this purpose, capillary pressures and relative permeabilities have to be measured for each sample that conformed the stack.

Experiment 2 showed the complexity caused by the presence of vugs in the rock sample. Similar experiments using rock samples with different levels of vuggy porosity can be performed in order to understand better the effect that this type of heterogeneity provokes in a naturally fractured reservoir under gravity drainage drive mechanism.

An execution of similar experiments of gravity drainage could be performed by creating a stack (as in experiment 1) of rock samples with different levels of secondary porosity. This type of experiment could mimic in a more realistic way the gravity drainage mechanism in naturally fractured reservoirs where secondary porosity is not constant throughout the reservoir.

Finally, similar experiments as the presented in this work may be performed in oil-wet rock samples to investigate the effect of wettability in gravity drainage for naturally fractured reservoirs.

REFERENCES

Akin, S. and Kovscek, A.R. 2003. Computed Tomography in Petroleum Engineering Research. *Geological Society, London, Special Publications* **215** (1): 23-38. doi: 10.1144/GSL.SP.2003.215.01.03.

Alvestad, J., Gilje, E., Hove, A.O. et al. 1992. Enhanced Oil Recovery Coreflood Experiments with Surfactant Systems for IOR: Computer Tomography Studies and Numerical Modelling. *Journal of Petroleum Science and Engineering* **7** (1): 155-71. doi: http://dx.doi.org/10.1016/0920-4105(92)90016-T.

Bech, N., Jensen, O.K. and Nielsen, B. 1991. Modeling of Gravity-Imbibition and Gravity-Drainage Processes: Analytic and Numerical Solutions. doi: 10.2118/18428-PA.

Beckner, B.L., Ishimoto, K., Yamaguchi, S. et al. 1987. Imbibition-Dominated Matrix-Fracture Fluid Transfer in Dual Porosity Simulators. doi: 10.2118/16981-MS.

Buckley, S.E. and Leverett, M.C. 1942. Mechanism of Fluid Displacement in Sands. doi: 10.2118/942107-G.

Cardwell, W.T., J. and Parsons, R.L. 1949. Gravity Drainage Theory. doi: 10.2118/949199-G.

Castelijns, J.H.P. and Hagoort, J. 1984. Recovery of Retrograde Condensate from Naturally Fractured Gas-Condensate Reservoirs. *Society of Petroleum Engineers Journal* doi: 10.2118/11199-PA.

Churcher, P.L., French, P.R., Shaw, J.C. et al. 1991. Rock Properties of Berea Sandstone, Baker Dolomite, and Indiana Limestone. doi: 10.2118/21044-MS.

Dykstra, H. 1978. The Prediction of Oil Recovery by Gravity Drainage. doi: 10.2118/6548-PA.

Firoozabadi, A. 1993. Some Recovery Issues of Immisible and Miscible Gas-Oil Flow in Fractured Reservoirs: Laboratory Data and Theoretical Analysys. *Proceedings on the First JNOC-TRC International Symposium on Carbonate Rocks-Hydrocarbon, Exploration and Reservoir Characterization* .

Firoozabadi, A. and Markeset, T. 1994. An Experimental Study of the Gas-Liquid Transmissibility in Fractured Porous Media. doi: 10.2118/24919-PA.

Firoozabadi, A. and Markeset, T. 1992. An Experimental Study of Capillary and Gravity Crossflow Fractured Porous Media. doi: 10.2118/24918-MS.

Hagoort, J. 1980. Oil Recovery by Gravity Drainage. *Society of Petroleum Engineers Journal* doi: 10.2118/7424-PA.

Hidajat, I., Mohanty, K.K., Flaum, M. et al. 2002. Study of Vuggy Carbonates using X-Ray CT Scanner and NMR. doi: 10.2118/77396-MS.

Izgec, O. and Hill, A.D. 2010. *Reactive flow in vuggy carbonates : methods and models applied ro matrix acidizing of carbonates. by Omer Izgec*: College Station, Tex.] : Texas A&M University], 2010].

Kazemi, H., Merrill, L.S., J., Porterfield, K.L. et al. 1976. Numerical Simulation of Water-Oil Flow in Naturally Fractured Reservoirs. doi: 10.2118/5719-PA.

Ketcham, R.A. and Carlson, W.D. 2001. Acquisition, Optimization and Interpretation of X-Ray Computed Tomographic Imagery: Applications to the Geosciences.

Computers & Geosciences **27** (4): 381-400. doi: http://dx.doi.org/10.1016/S0098-3004(00)00116-3.

Ladron, d.G., Rodriguez-de, l.G. and Galindo-Nava, A. 2009. Gravity-Drainage and Oil-Reinfiltration Modeling in Naturally Fractured Reservoir Simulation. doi: 10.2118/108681-PA.

Litvak, B.L. 1985. Simulation and Characterization of Naturally Fractured Reservoirs. *paper presented at the Reservoir Characterization Technical Conference, Dallas, TX*.

London, M., Cameron, S.M., Donald, J. et al. 2014. Waterflooding Experiments with X-Ray CT Imaging. doi: 10.2118/170147-MS.

Luan, Z. 1994. Some Theoretical Aspects of Gravity Drainage in Naturally Fractured Reservoirs. doi: 10.2118/28641-MS.

MacAllister, D. J., Miller, K. C., Graham, S. K., & Yang, C.-T. (1993, September 1). Application of X-Ray CT Scanning To Determine Gas/Water Relative Permeabilities. Society of Petroleum Engineers. doi:10.2118/20494-PA

McCain, W.D. 1990. *The properties of petroleum fluids. 2nd ed. William D. McCain, Jr*: Tulsa, Okla. : PennWell Books, 1990]; 2nd ed.

Miguel-H, N., Miller, M.A. and Sepehrnoori, K. 2004. Scaling Parameters for Characterizing Gravity Drainage in Naturally Fractured Reservoirs. doi: 10.2118/89990-MS.

Moctezuma-Berthier, A. and Fleury, M. 2000. Permeability Mapping on Vuggy Core Sample Using Tracer Experiments and Stream-Line Simulations. doi: 10.2118/58992-MS.

Mohan, K.K., Vaidya, R.N., Reed, M.G. et al. 1993. Water sensitivity of sandstones containing swelling and non-swelling clays. *Colloids and Surfaces A: Physicochemical and Engineering Aspects* : 237-254.

Pavone, D., Bruzzo, P. and Verre, R. 1989. Gravity Drainage at Low Interfacial Tension. *5th European Symposium on Enhanced Oil Recovery* .

Potts, D.E. and Kuehne, D.L. 1988. Strategy for Alkaline/Polymer Flood Design With Berea and Reservoir-Rock Corefloods. doi: 10.2118/14935-PA.

Quandalle, P. and Sabathier, J.C. 1989. Typical Features of a Multipurpose Reservoir Simulator. doi: 10.2118/16007-PA.

Rangel-German, E.R. and Kovscek, A.R. 2002. Experimental and analytical study of multidimensional imbibition in fractured porous media. *Journal of Petroleum Science and Engineering* **36** (1–2): 45-60. doi: http://dx.doi.org/10.1016/S0920-4105(02)00250-4.

Schechter, D.S. and Guo, B. 1996. Mathematical Modeling of Gravity Drainage After Gas Injection into Fractured Reservoirs. doi: 10.2118/35170-MS.

Sonier, F., Souillard, P. and Blaskovich, F.T. 1988. Numerical Simulation of Naturally Fractured Reservoirs. doi: 10.2118/15627-PA.

Van Geet, M., Swennen, R. and Wevers, M. 2001. Towards 3-D petrography: application of microfocus computer tomography in geological science. *Computers &*

Geosciences **27** (9): 1091-9. doi: http://dx.doi.org/10.1016/S0098-3004(00)00154-0.

Vinegar, H.J. and Wellington, S.L. 1987. Tomographic Imaging of Three-Phase Flow Experiments. *Review of Scientific Instruments* .

Wellington, S.L. and Vinegar, H.J. 1987. X-Ray Computerized Tomography. doi: 10.2118/16983-PA.

Withjack, E.M. 1988. Computed Tomography for Rock-Property Determination and Fluid-Flow Visualization. doi: 10.2118/16951-PA.